Analysis of non-derivatized bacteriohopanepolyols using UHPLC-HRMS reveals great structural diversity in environmental lipid assemblages

HOPMANS, Ellen C, SMIT, Nadine T, SCHWARTZ-NARBONNE, Rachel <http://orcid.org/0000-0001-9639-9252>, SINNINGHE DAMSTÉ, Jaap S and RUSH, Darci

Published version

HOPMANS, Ellen C, SMIT, Nadine T, SCHWARTZ-NARBONNE, Rachel, SINNINGHE DAMSTÉ, Jaap S and RUSH, Darci (2021). Analysis of non-derivatized bacteriohopanepolyols using UHPLC-HRMS reveals great structural diversity in environmental lipid assemblages. Organic Geochemistry, p. 104285.

Journal Pre-proofs

Analysis of non-derivatized bacteriohopanepolyols using UHPLC-HRMS reveals great structural diversity in environmental lipid assemblages

Ellen C. Hopmans, Nadine T. Smit, Rachel Schwartz-Narbonne, Jaap S. Sinninghe Damsté, Darci Rush

PII: S0146-6380(21)00106-6
DOI: https://doi.org/10.1016/j.orggeochem.2021.104285
Reference: OG 104285

To appear in: *Organic Geochemistry*

Received Date: 22 April 2021
Revised Date: 8 July 2021
Accepted Date: 14 July 2021

Please cite this article as: Hopmans, E.C., Smit, N.T., Schwartz-Narbonne, R., Sinninghe Damsté, J.S., Rush, D., Analysis of non-derivatized bacteriohopanepolyols using UHPLC-HRMS reveals great structural diversity in environmental lipid assemblages, *Organic Geochemistry* (2021), doi: https://doi.org/10.1016/j.orggeochem.2021.104285

Analysis of non-derivatized bacteriohopanepolyols using UHPLC-HRMS reveals great structural diversity in environmental lipid assemblages

Ellen C. Hopmans[1*], Nadine T. Smit[1], Rachel Schwartz-Narbonne[2], Jaap S. Sinninghe Damsté[1,3], Darci Rush[1,2]

[1]NIOZ Royal Institute for Sea Research, Department of Marine Microbiology and Biogeochemistry, P.O. Box 59, 1790 AB Den Burg, Texel, The Netherlands

[2]School of Natural and Environmental Sciences, Newcastle University, Newcastle upon Tyne, NE1 7RU, United Kingdom

[3]Utrecht University, Faculty of Geosciences, Department of Earth Sciences, P.O. Box 80.121, 3508 TA Utrecht, the Netherlands

[*] Corresponding author: ellen.hopmans@nioz.nl

Running Title: Analysis of non-derivatized bacteriohopanepolyols

Keywords: non-derivatized bacteriohopanepolyols, UHPLC-HRMS, novel composite BHPs, adenosylhopanes

Abstract

Bacteriohopanepolyols (BHPs) are lipids with great chemotaxonomic potential for microbial populations and biogeochemical processes in the environment. The most commonly used methods for BHP analysis are chemical degradation followed by gas chromatography-mass spectrometry (MS) or derivatization followed by high performance liquid chromatography (HPLC)- atmospheric pressure chemical ionization/MS. Here we report on significant advances in the analysis of non-derivatized BHPs using U(ltra)HPLC-electrospray ionization-high resolution MS^2. Fragmentation mass spectra provided information on the BHP core, functionalized side chain, as well as the conjugated moiety of composite BHPs. We successfully identified the common bacteriohopanepolyols and their (di)methylated and (di)unsaturated homologues, aminoBHPs, and composite BHPs (e.g., cyclitol ethers and methylcarbamateBHPs) in biomass of several known BHP-producing micro-organisms. To show how the method can be exploited to reveal the diversity of BHPs in the environment, we investigated a soil from an active methane seep, in which we detected ca. 130 individual BHPs, including a complex distribution of adenosylhopanes. We identified the nucleoside base moiety of both adenosylhopane type-2 and type-3. Adenosyl hopane type-3 contains a methylated adenine as its nucleobase, while type-2 appears to contain a deaminated and methylated adenine, or N1-methylinosine. In addition, we detected novel adenosylhopanes. Furthermore, we identified a novel series of composite BHPs comprising of bacteriohopanepolyols conjugated to an ethenolamine moiety. The novel ethanolamineBHPs as well as aminoBHPs were also detected acylated to fatty acids. The analytical approach described allows for simultaneous analysis of the full suite of IPLs, now including BHPs, and represents a further step towards environmental lipidomics.

1. Introduction

Bacteriohopanepolyols (BHPs) are membrane lipids with great chemotaxonomic potential with regards to microbial populations as well as biogeochemical processes in the environment. BHPs are composed of a pentacyclic triterpenoid ring system with an extended side chain containing 4, 5, or 6 functional groups (Fig. S1) comprised of either all hydroxyl moieties (bacteriohopanetetrol (BHT), bacteriohopanepentol (BHpentol), and bacteriohopanehexol (BHhexol); Rohmer et al., 1984; Talbot et al., 2003a; Talbot and Farrimond, 2007) or 3, 4, or 5 hydroxyl moieties and a single terminal amino-group (i.e., aminotriol, -tetrol, and -pentol; e.g., Neunlist and Rohmer, 1985b; Rohmer, 1993). The basic, unmodified ring system with a linear side chain is usually the dominant BHP in both culture and environmental samples (see also review of BHP sources in Talbot and Farrimond, 2007, and Talbot et al., 2008). BHPs can be further modified by methylation at the C-2 (2MeBHPs; e.g., Talbot et al., 2008 and references therein), C-3 (3MeBHPs; e.g., Cvejic et al., 2000a), both C-2 and C-3 (2,3diMeBHPs; Sinninghe Damsté et al., 2017), C-31 (Simonin et al., 1994), or C-12 (Costantino et al., 2000) positions. BHPs can also include unsaturation in the ring system located at Δ^6, Δ^{11} or both (Talbot et al., 2007b and references therein). A BHP with an unsaturation in the side chain was identified in a methanotrophic *Methylovulum* bacterium (van Winden et al., 2012). A large variety of so-called composite BHPs, where the terminal functional group is bound to complex, often polar moieties, have also been identified (Talbot et al., 2007a and references therein), such as the adenosylhopanes, acylated BHPs, and cyclitol ether BHPs (BHP-CE). BHPs with novel side chains are continually being discovered (e.g., Kool et al., 2014; Rush et al., 2016). The diverse nature of BHP lipid structures has lead to particular BHPs being used as biomarkers for unique bacterial source organisms (van Winden et al., 2012; Kool et al., 2014; Rush et al., 2014), environmental

conditions (Ricci et al., 2014; Welander and Summons, 2012), and organic matter origin (Zhu et al., 2011).

The first reports of BHPs in the natural environments were based on analysis with gas chromatography coupled to mass spectrometry (GC-MS; Rohmer et al., 1980). Traditionally, the GC-MS identification and quantification of BHPs in organic extracts are based on a degradation with periodic acid which converts the intact BHPs into $C_{30} - C_{32}$ primary alcohols, followed by acetylation. Analyses of these derivatised hopanols provide information about the number of functional groups present in the original intact molecule (Rohmer et al., 1984). The analysis of hopanoids by way of GC-MS has been a big step forward in understanding the distribution of BHPs in modern systems and the geological archive. However, by removing all but one functional group from the side chain using the Rohmer reaction, much of the source-, environment-, or process-specific information is lost. In addition to this being a laborious method, it is also completely unable to detect composite BHPs, leading to potential underestimation of BHP abundance and complexity. To fully elucidate the array of BHP structures, alternative methodologies have been developed. In 2013, Sessions et al. published a high temperature (HT)GC-MS method that achieves elution and separation of more complex acetylated intact BHPs on two different GC columns (BHT, BHpentol and aminotriol on DB-5HT; 2MeBHPs on DB-XLB stationary phase). Though HTGC-MS shows promise, the vast majority of work on intact BHPs, however, has been performed using HPLC-MS.

Schulenberg-Schell et al. (1989) developed a reversed phase HPLC method for analysis of BHPs after acetylation. This method was modified by Talbot et al. (2001), where its applicability was demonstrated in a study of the BHP profiles from a group of methanotrophic bacteria. Advances followed with the application of atmospheric pressure chemical ionization (APCI)/ion trap multi-stage MS, which allowed for more precise control of the fragmentation

of the precursor ions. Since 2003, most environmental and culture studies of BHPs have used a version of this reversed phase chromatographic method (e.g., Blumenberg et al., 2007; Saenz et al., 2011; Talbot et al., 2003a, b). The subsequent investigation of a wider range of hopanoid-producing bacterial cultures (Talbot et al., 2003b, c; Talbot et al., 2007a, b; Talbot et al., 2008) led to the improved understanding of the fragmentation pathways in a greater diversity of BHP structures. This allowed for the identification of known BHPs, and related unknown BHPs (e.g., van Winden et al., 2012, Rush et al., 2016). Recently, several studies were published successfully applying ultra high pressure liquid chromatography (UHPLC) for improved separation of acetylated BHPs (Kusch et al., 2018, Hemingway et al., 2018), especially isomers of BHT.

The analysis of derivatised BHPs using HPLC-MS has its own disadvantages. The acetylation efficiencies of individual BHPs vary and some BHPs, e.g., BHT-CE, acetylate incompletely resulting in the production of several acetylomers complicating data interpretation. Also, as is the case in general for HPLC-MS analysis, response factors are different for different BHPs making quantitation difficult. With the introduction of improved UHPLC-MS instruments and advances in the quality and diversity of the stationary phases, it became possible to introduce improved methods for analyzing non-derivatised BHPs. Based on an application note (Isaac et al., 2011), non-derivatised BHPs were successfully identified in bacterial isolates and purified culture material using a UHPLC-tandem MS system (Malott et al. 2014; Wu et al, 2015) but these studies did not show the comprehensiveness and sensitivity necessary to cover a wide range of BHPs. Malott et al. (2014) did not report BHPs known to be synthesised by their investigated organism (i.e., BHT and unsaturated BHT-CE in *Burkholderia* spp. (Cvejic et al., 2000b) and Wu et al. (2015) reported a reduction in ionization efficiencies of non-acetylated BHPs compared to their acetylated counterparts. Recently, Talbot et al. (2016) reported on the development of an UHPLC method coupled to APCI/triple Quadrupole MS in multi reaction

monitoring (MRM) mode for non-derivatized BHPs. However, this work remained limited to a restricted number of already identified BHPs.

Here we report on significant advances in the analysis of non-derivatized BHPs using UHPLC coupled to electrospray ionization (ESI)-high resolution dual-stage MS ($HRMS^2$). Using an approach, which has been successfully applied to the analysis of intact polar lipids (IPLs), we analyzed a number of bacterial species, a.o. '*Candidatus* Scalindua profunda', '*Ca.* Methylomirabilis oxyfera', *Methylococcus capsulatus*, and *Methylomarinum vadi*, as well as a soil from an active terrestrial methane seep. We discuss elution and fragmentation behaviour of a wide range of known BHPs, including N-containing BHPs and composite BHPs, and the tentative identification of an extensive set of novel BHPs.

2. Materials and Methods

2.1 Sample description

Komagataeibacter xylinus strain R-2277 (formerly *Gluconacetobacter xylinus* and *Acetobacter aceti* ssp. *xylinum*) was obtained as frozen cells in culture medium from an industrial culture (Hoffmann-La Roche, Basel). This culture has been used in previous BHP studies (Peiseler and Rohmer, 1992; Schwartz-Narbonne et al., 2020). An enrichment culture of the bacterium '*Ca.* Methylomirabilis oxyfera' was obtained from a bioreactor operated under conditions described previously by Ettwig et al. (2009). The bioreactor population consisted of ca. 67% '*Ca*. M. oxyfera', while the remainder was composed of a mix of ANME-2d archaea and different minor bacteria phyla (see Smit et al. (2019) for details). This culture has been used in previous BHP studies by Kool et al. (2014). *Methylococcus capsulatus* (strain Bath) was obtained from the University of Warick culture collection (as described in Talbot et al., 2001). *M. capsulatus* has been studied in previous BHP studies by

Neunlist and Rohmer (1985b) and Talbot et al. (2001). An enrichment culture of '*Ca.* Scalindua profunda' was grown in a sequencing batch reactor at room temperature (ca. 20 °C) as described by van de Vossenberg et al. (2008) and consisted of 80-90% '*Ca.* S. profunda'. BHPs have been previously studied in this ongoing enrichment culture by Rush et al. (2014) and Schwartz-Narbonne et al. (2020). *Methylomarinum vadi* (strain IT-4) was isolated from a microbial mat of a shallow (~23 m water depth) marine hydrothermal system in a coral reef off Taketomi Island, Okinawa, Japan (Hirayama et al., 2007; 2013). Cultivation of this strain was performed at JAMSTEC, Japan, using MJmet mediumat pH 6.6 at 37 °C. This culture has been used in previous BHP studies (Rush et al., 2016).

The Fuoco di Censo seep (37°37'30.1''N, 13°23'15.0''E), in the mountains of Southwestern Sicily, Italy, is a typical example of a natural 'Everlasting Fire' (Etiope et al., 2002; Grassa et al., 2004; Smit et al., 2021). The Censo seep gas consists of mainly thermally generated methane (76-86%). A soil sample was recovered from a horizon 5-10 cm below soil surface directly at the main gas seep (Censo 0 m). The soil sample was stored in a clean geochemical sampling bag and kept frozen at -20 °C until freeze drying and extraction. Further details can be found in Smit et al. (2021).

2.2 Lipid extraction

Freeze-dried bacterial biomass and the soil from the Censo seep were extracted using a modified Bligh and Dyer method (Bligh and Dyer, 1959; Bale et al., 2013). The samples were ultrasonically extracted (10 min) with a solvent mixture containing methanol (MeOH), dichloromethane (DCM) and phosphate buffer (2:1:0.8, v:v:v). Solvent was collected after centrifugation and the residues re-extracted twice. A biphasic separation was achieved by adding additional DCM and phosphate buffer to the combined extracts in a ratio of MeOH,

DCM and phosphate buffer (1:1:0.9, v:v:v). After the DCM layer was collected, the aqueous layer was washed twice with DCM. Combined DCM layers were dried under a continuous flow of N_2. Prior to injection, extracts were redissolved in MeOH:DCM (9:1) and filtered through a 0.45 µm regenerated cellulose syringe filter (4 mm diameter; Grace Alltech, Deerfield, IL).

2.3 UHPLC/HRMS

The method described here (adapted from Wörmer et al., 2013) is the final method used. Steps in method development are discussed below in Results and Discussion. All analyses were performed using an Agilent 1290 Infinity I UHPLC, equipped with thermostatted autosampler and column oven, coupled to a quadrupole-orbitrap HRMS equipped with an Ion Max source and heated ESI probe (HESI) (ThermoFisher Scientific, Waltham, MA). Separations were achieved using an Acquity C_{18} BEH column (2.1x 150 mm, 1.7 µm particle; Waters), fitted with a pre-column, and a solvent system consisting of (A) methanol:H_2O (85:15) and (B) methanol:isopropanol (1:1), both containing 0.12% (v/v) formic acid and 0.04% (v/v) aqueous ammonia. Compounds were eluted with 5% B for 3 min, followed by a linear gradient to 40% B at 12 min and then to 100% B at 50 min, with a total run time of 80 min. The flow rate was 0.2 mL min^{-1}. Positive ion HESI settings were: capillary temperature, 300 °C; sheath gas (N_2) pressure, 40 arbitrary units (AU); auxiliary gas (N_2) pressure, 10 AU; spray voltage, 4.5 kV; probe heater temperature, 50 °C; S-lens 70 V. Detection was achieved using positive ion monitoring of *m/z* 350-2000 (resolution 70,000 ppm at *m/z* 200), followed by data dependent MS^2 (isolation window 1 *m/z*; resolution 17,500 ppm at *m/z* 200) of the 10 most abundant ions (total cycle time ca. 1.2 s), and dynamic exclusion (6 s) with 3 ppm mass tolerance. In addition, an inclusion list of 165 calculated exact masses of BHPs from literature

was used. Optimal fragmentation of BHPs was achieved using a stepped normalized collision energy of 22.5 and 40. A mass calibration was performed every 48 h using the Thermo Scientific Pierce LTQ Velos ESI Positive Ion Calibration Solution. All mass chromatograms were produced within 3 ppm mass accuracy, unless otherwise stated.

3. Results and Discussion

3.1 UHPLC method development

The suitability of C_{18} columns for the retention and separation of several non-derivatized BHPs was previously demonstrated by Talbot et al. (2016). Two types of C_{18} column were tested in that study: an Acquity BEH UHPLC column and an Ace base-deactivated Excel UHPLC column, of which the latter showed the best chromatographic behavior, particularly for N-containing BHPs. Previously, the Acquity BEH C_{18} column was selected by Wörmer et al. (2013) in a new UHPLC-ESI/MS method for the analysis of IPLs. As BHPs, like IPLs, consist of a large apolar moiety and a polar functionalized side chain with or without an additional, often polar, moiety or head group, we set out to test whether the chromatographic system, combined with positive ion ESI, as described by Wörmer et al. (2013) for IPLs, is suitable for the analysis of non-derivatized BHPs. For this purpose, we investigated extracts of biomass of various known BHP-producing bacteria. The exact distribution of the detected BHPs and their fragmentation spectra are discussed in detail in section 3.3. Here we only discuss the general features of the chromatographic method. BHT was easily identified in several extracts based on its exact mass and diagnostic spectra. Aminotriol and -tetrol produced very broad peaks and were thus difficult to detect, similarly as was described by Talbot et al. (2016). The buffering system according to Wörmer et al. (2013) consists of 0.04% formic acid and 0.1% NH_3, producing a mobile phase with pH 6. The pH is often a

driving factor in the chromatographic behavior of N-containing compounds and therefore a more acidic buffering system with 0.12% formic acid and 0.04% NH_3, which has also been frequently used in IPL HPLC-MS analysis (cf. Sturt et al., 2004), was tested. This change in the pH of the mobile phase to 4 resulted in excellent peak shape for the N-containing BHPs using the Acquity BEH C_{18} column, allowing detection of e.g., aminotriol and -tetrol, as well as adenosylhopane BHPs. Use of the base deactivated Ace Excel C_{18} column in combination with the mobile phase with pH 4 did not result in improved chromatography and thus, for all experiments described below, a combination of the Acquity BEH C_{18} column combined with the pH 4 buffering system was used.

3.2 MS method development

MS detection of derivatized BHPs, in general, has been done by using positive ion APCI combined with ion trap MS^2 (Talbot et al. 2003a, b, 2007a, b). For non-derivatized BHPs, Talbot et al. (2016) employed APCI combined with MRM using a triple quadrupole MS. Here we explored the use of positive ion ESI combined with a quadrupole-Orbitrap MS for untargeted detection and identification of BHPs with data dependent MS^2 analysis using HRMS, similar to the approach that has successfully been applied to the analysis of IPLs (Moore et al., 2016; Besseling et al., 2018; Bale et al., 2019). For non-targeted IPL analysis we apply a stepped normalized collision energy of 15, 22.5 and 30 to produce informative and diagnostic spectra (e.g., Bale et al., 2018; Sollai et al., 2018). For relatively simple BHPs, such as BHT, BHpentol and BHhexol, these settings resulted in good quality MS^2 spectra, but especially for N-containing BHPs such as aminotriol and -tetrol it gave insufficient fragmentation to obtain an informative MS^2 spectrum. Talbot et al. (2016) also reported the necessity for a higher fragmentation energy for the N-containing BHPs. However, exploring this option led to the MS^2 spectra of non N-containing BHPs having too much fragmentation,

and thus loss of information on the structure of the side chains. A workable compromise was achieved by using a stepped normalized collision energy of 22.5 and 40, resulting in MS^2 spectra with diagnostic losses for the different possible functional groups in the tail and diagnostic fragmentation for the hopanoid core. All fragmentation spectra discussed below were produced using these settings.

3.3. Commonly detected BHPs in various microorganisms

Talbot et al. (2016) reported MS^2 spectra under various fragmentation conditions for non-derivatized BHT. However, no spectra were reported for methylated BHTs, unsaturated BHTs or BHpentol and BHhexol. To establish the chromatographic behavior and fragmentation of various BHPs we analyzed biomass of several known BHP-producing bacteria.

3.3.1. Bacteriohopanetetrols.

Biomass of *K. xylinus,* which has been reported to produce multiple (3Me)BHT isomers with up to two unsaturations at Δ^6 and/or Δ^{11} (Peisler and Rohmer,1992, Talbot et al., 2007b), was analyzed to study the various isomers and homologues of BHT. Schwartz-Narbonne et al. (2020) already showed the separation of different stereoisomers of non-derivatized BHTs (i.e., BHT-34*S*, BHT-34*R* and BHT-x) using the method described here. Analysis of biomass of *K. xylinus* provided further evidence that various stereoisomers of BHT are (partially) separated under the UHPLC conditions in this study (Fig. 1). Table S1 lists all BHPs discussed below and provides details on preferred ionization, in-source fragmentation and diagnostic fragments.

The summed mass chromatogram of the calculated exact masses of the protonated ($[M+H]^+$), ammoniated ($[M+NH_4]^+$) and sodiated molecules ($[M+Na]^+$) of BHT (*m/z* 547.472, *m/z* 564.499, *m/z* 569.454, respectively) revealed the presence of multiple isomers of BHT (Fig.

1A). The two peaks at 20.8 and 21.1 min (peaks b and c) match the retention time for BHT with the 22*R*,34*S* and 22*R*,34*R* stereochemistry, respectively, as established by Schwarz-Narbonne et al. (2020). The most abundant isomer of BHT (i.e., labeled a), eluting early at 19.3 min, may be BHT-22*S*,34*S*, which was reported in relatively high abundance (13% of all BHTs) in *K. xylinus* by Peiseler and Rohmer (1992). In addition to these abundant isomers, there are several isomers present at trace levels (not visible at the scale of Fig. 1) eluting after both the early eluting BHT isomer and the BHT-22*R*,34*S*/*R*.

All the BHT isomers described above had similar MS^2 spectra, therefore we only discuss the MS^2 spectrum of BHT-22*R*,34*S* (peak b, Fig. 1A), obtained from the ammoniated molecule (*m/z* 564.5; Fig. 2A). The MS^2 spectrum obtained here is similar to that reported by Talbot et al. (2016) for non-derivatized BHT upon MS^2 fragmentation of *m/z* 529 (formed after in source loss of H_2O from protonated BHT ($[M+H-H_2O]^+$)). Here, *m/z* 529.461 ($C_{35}H_{61}O_3^+$, Δ ppm -0.65) is the base peak. Fragment ions at *m/z* 511.450 ($C_{35}H_{59}O_2^+$, Δ ppm -1.56), *m/z* 493.437 ($C_{35}H_{57}O^+$, Δ ppm -6.73), and *m/z* 475.430 ($C_{35}H_{55}^+$, Δ ppm -0.80) represent consecutive losses of hydroxyl moieties as H_2O (see Table S1 for assigned elemental composition (AEC) of fragments). In the lower mass range, *m/z* 163.148 ($C_{12}H_{19}^+$, Δ ppm -0.17) is the dominant fragment, but the universal diagnostic fragment ion for hopanoids (*m/z* 191.179, $C_{14}H_{23}^+$, Δ ppm -0.56) (Peters and Moldowan, 1993) is clearly present and more dominant than observed in the spectrum of Talbot et al. (2016). Unlike electron ionization (EI) fragmentation, collision-induced dissociation (CID) fragmentation typically does not produce radicals but one protonated fragment and a neutral. Any cleavage results in proton rearrangements and the formation of a double bond equivalent in one of the two fragments (for discussed fragmentation pathways and fragments, see Fig. 3). In case of BHT, the *m/z* 191 fragment represents the protonated A and B ring of the hopanoid structure with 2 double bonds (unlike the structure proposed by Talbot et al. (2003b)), generated by the double

cleavage at C-9/C-11 and C-8/C-14 following fragmentation pathway A. Additional diagnostic fragments are found at *m/z* 369.352 (complete hopanoid ring system after loss of side chain; $C_{27}H_{45}^+$, Δ ppm -0.21) and at *m/z* 283.242 ($C_{21}H_{31}^+$, Δ ppm -1.58), *m/z* 301.251 ($C_{21}H_{33}O^+$, Δ ppm -3.63), 319.264 ($C_{21}H_{35}O_2^+$, Δ ppm 3.52), and 337.273 ($C_{21}H_{37}O_3$+, Δ ppm -1.19). These latter C_{21} fragments are complementary to the fragment at *m/z* 191 and represent the D and E rings and side chain with 0 to 3 alcohol moieties remaining (fragmentation A', Fig. 3). Talbot et al. (2003a, b) observed the equivalent fragments for acetylated BHT.

3.3.2 Methylated BHTs.

The distribution of the 3MeBHTs in *K. xylinus* in general followed the distribution of the BHTs and they elute roughly 2 min after their non-methylated BHT-counterparts, but were ca. an order of magnitude less abundant. Two stereoisomers of 3MeBHT were detected (peaks k and l, Fig. 1D) and based on their relative retention time were identified as 3MeBHT-22*R*,34*S* and 3MeBHT-22*R*,34*R*, respectively. Peiseler and Rohmer (1992) reported only the 3MeBHT-22*R*,34*S* in *K. xylinus,* but did observe the *22R*,34*R* stereoisomer in the acetic acid bacterium *A. pasteurianus.* The MS^2 spectra (Fig. S2A) showed the expected offset of +14 Da in the fragments containing the A ring with the methylation (e.g., *m/z* 177.164 ($C_{13}H_{21}^+$, Δ ppm -0.55), *m/z* 205 ($C_{15}H_{25}^+$, Δ ppm -0.33), *m/z* 219 ($C_{16}H_{27}^+$, Δ ppm -0.40) and *m/z* 383 ($C_{28}H_{47}$, Δ ppm 1.52), while fragments related to the D and E rings with side chain did not show the offset (e.g., *m/z* 283.242 ($C_{21}H_{31}^+$, Δ ppm 1.21), *m/z* 301.253 ($C_{21}H_{35}O^+$, Δ ppm 1.86), *m/z* 319.263 ($C_{21}H_{35}O_2^+$, Δ ppm 0.48), *m/z* 337.274 ($C_{21}H_{37}O_3^+$, Δ ppm -0.54).

K. xylinus does not produce 2MeBHTs. Both acetylated and non-derivatized 2MeBHPs elute very closely after their non-methylated counterparts using reversed phase chromatography, while 3MeBHPs elute later (Talbot et al. 2003a, b; 2007a, b; 2016). Based on this elution pattern, we detected 2MeBHT in a soil nearby a methane seep (discussed in section 3.5 and further) of which all identified BHPs are listed in Table S2.

3.3.3. Unsaturated BHTs.

We also detected several isomers of unsaturated BHTs in biomass of *K. xylinus* (Fig. 1B). The summed mass chromatogram of the calculated exact masses of the protonated, ammoniated, and sodiated molecules of unsaturated BHT (*m/z* 545.456 + 562.483 + 567.438) showed two main peaks at 18.5 and 18.7 min (e and f), as well as a minor early eluting isomer at 17.8 min (d) and a pair of late eluting isomers at 19.5 and 19.6 min (g and h). Peiseler and Rohmer (1992) reported two isomers of Δ^6-BHT (22*R*,34*S* and 22*R*,34*R*) in relatively high abundance in *K. xylinus* (20 and 36% respectively of total BHTs). Based on this distribution it is likely that peaks e and f represent Δ^6-BHT-22*R*,34*S* and Δ^6-BHT-22*R*,34*R*, respectively. The MS^2 spectra of the ammoniated molecules (*m/z* 562.5) associated with peaks e and f (e.g., Fig. 2B) are almost identical. The HPLC-MS^2 analysis of acetylated unsaturated BHTs was extensively discussed by Talbot et al. (2007b), but not for non-derivatized BHTs (Talbot et al. 2016). The unsaturation in Δ^6-BHT-22*R*,34*R* (peak f, Fig. 2B) is clearly observed in several fragments formed after consecutive losses of H_2O from the side chain, that are offset by 2 Da from the spectrum of BHT, e.g., *m/z* 527.466 ($C_{35}H_{59}O_3^+$, Δ ppm -0.36), 509. 435 ($C_{35}H_{57}O_2^+$, Δ ppm -0.37), 491.421 ($C_{35}H_{55}O^+$, Δ ppm -6.76) and 473.415 ($C_{35}H_{53}^+$, Δ ppm 1.88). Interestingly, and similar as described by Talbot et al. (2007), no such offset is observed in the diagnostic fragment ion at *m/z* 191.179 ($C_{14}H_{23}^+$, Δ ppm -0.88). While in case of BHT the fragment at *m/z* 191 is produced by cleavage at C-9/C-11 and C-8/C-14 and a proton rearrangement resulting in two double bonds in the A and B Ring fragment (as discussed above), it appears that the presence of a pre-existing double bond at Δ^6 results in an alternative proton rearrangement; only one additional double bond is formed in the A and B ring fragment, thus generating the *m/z* 191 also seen in BHT, and the other double bond is formed in the neutral loss fragment (fragmentation A, Fig. 3). Talbot et al. (2007b) also observed evidence for an alternative fragmentation pathway in acetylated Δ^6-BHT, with cleavage of the C-11/C-12 and

C-8/C-14 bonds (pathway B, Fig. 3). With proton rearrangement to form two additional double bonds on the A and B ring fragment, this fragmentation would produce the here observed *m/z* 203.179 ($C_{15}H_{23}^+$, Δ ppm -0.233; Fig. 3). A complementary series of C_{20} fragments with 1-3 hydroxyl moieties are observed at *m/z* 287.237 ($C_{20}H_{31}O^+$, Δ ppm 0.41), 305.247 ($C_{20}H_{33}O_2^+$, Δ ppm -0.42) and 323.258 ($C_{20}H_{35}O_3^+$, Δ ppm -0.44) and represent the D and E rings with the (partially dehydroxylated) side chain.

The MS^2 spectra of peaks g and h (Fig. 1B) are largely similar to those of peaks d-f, however there are some notable differences in the middle mass range (Fig. 2C), which shows a series of C_{20} to C_{28} fragments with up to three hydroxyl moieties. It is possible that the presence of a double bond in the C ring leads to a multitude of alternative fragmentation pathways involving the A and B rings. For example, the larger fragments (>C_{24}) appear to originate from cleavage of the C-9/C-10 bond in combination with cleavage at C-5/C-6, C-6/C-7, or C-7/C-8 (Fig. 3, pathways C, D, E). We, therefore, tentatively assign the location of the unsaturation in peaks g and h to Δ^{11}. Peiseler and Rohmer (1992) did not report Δ^{11}-BHT in *K. xylinus*, perhaps due to lesser sensitivity of the method used, however both Δ^{11}-3MeBHT-22*R*,34*S* and Δ^{11}-3MeBHT-22*R*,34*R* were reported in this microorganism, showing its capability to produce an unsaturation at that position. Based on this and the typical pair-wise elution pattern observed here for the 22*R*,34*S* and 22*R*,34*R* stereoisomers of BHT and Δ^6-BHT, we tentatively identify peaks g and h as Δ^{11}-BHT-22*R*,34*S* and Δ^{11}-BHT-22*R*,34*R*.

The MS^2 spectrum of the early eluting isomer (d) is almost identical to those of peaks e and f (Δ^6-BHT-22*R*,34*S* and Δ^6-BHT-22*R*,34*R)*, suggesting that this isomer contains a double bond at Δ^6. If that is the case, and based on the retention time offset between the BHT-22*R*,34*S*/*R* pair and the Δ^6-BHT-22*R*,34*S*/*R* pair, its fully saturated BHTcounterpart would be one of the very minor BHT isomers with unknown stereochemistry eluting between peaks a and b.

The summed mass chromatogram revealing the distribution of di-unsaturated BHTs (Fig. 1C) shows two main peaks at 17.5 and 17.7 min (peaks i and j), most likely the 34*S* and 34*R* stereoisomers of $\Delta^{6,11}$-BHT as described by Peiseler and Rohmer (1992). MS^2 spectra of the ammoniated molecule of di-unsaturated BHTs (*m/z* 560.5, Fig. 2D) reveal double unsaturations in the fragments that result from the loss of hydroxyl moieties from the side chain (e.g., *m/z* 525.430 ($C_{35}H_{57}O_3^+$, Δ ppm 0.03), *m/z* 507.419 ($C_{35}H_{55}O_2^+$, Δ ppm -0.98), and *m/z* 489.410 ($C_{35}H_{53}O^+$, Δ ppm 1.61)). However, the MS^2 is dominated by fragments at *m/z* 119.086 ($C_9H_{11}^+$, Δ ppm 0.03) and *m/z* 189.164 ($C_{14}H_{21}^+$, Δ ppm -0.36), similar to what was observed by Talbot et al. (2007b) for MS^2 spectra of acetylated di-unsaturated BHT. Rohmer and Ourison (1986) attributed a fragment at m/z 119, formed after EI from both Δ^6- and $\Delta^{6,11}$-BHPs, to the B-ring and assigned a trimethylbenzene structure. However, a trimethylbenzene would yield, if protonated, a fragment at *m/z* 121 ($C_9H_{13}^+$) and thus is seems the fragment at *m/z* 119 formed upon CID fragmentation, represents a different, and as yet unknown, fragment. The fragment at *m/z* 189 likely represents the A and B rings. Although formation of an A and B ring fragment with three double bonds does not appear to be favored in case of a Δ^6 -unsaturation, an additional unsaturation at Δ^{11} apparently forces this proton rearrangement, thus producing a fragment at *m/z* 189 (pathway A, Fig. 3). It is therefore important to recognize that with CID, *m/z* 189 is not diagnostic for a Δ^6-unsaturation (as is the case with EI fragmentation), but instead indicates a $\Delta^{6,11}$ -unsaturation. The fragments in the middle mass range in the MS^2 spectrum of the di-unsaturated BHT are less abundant (<2%; e.g. *m/z* 257.266 ($C_{19}H_{29}^+$, Δ ppm -0.38), *m/z* 269.226 ($C_{20}H_{29}^+$, Δ ppm -0.08), *m/z* 283.242 ($C_{21}H_{31}^+$, Δ ppm -1.65), *m/z* 319.264 ($C_{21}H_{35}O_2^+$, Δ ppm 2.08), *m/z* 337.274 ($C_{21}H_{37}O_3^+$, Δ ppm 1.77), *m/z* 389.305 ($C_{25}H_{41}O_3^+$, Δ ppm 1.10), *m/z* 415.321 ($C_{27}H_{43}O_3^+$, Δ ppm 0.21), *m/z* 429.336 ($C_{28}H_{45}O_3^+$, Δ ppm 0.02), *m/z* 441.336 ($C_{29}H_{45}O_3^+$, Δ ppm 0.29)) and appear to represent a combination of the fragment pathways observed for the Δ^6- and Δ^{11}-unsaturation.

3.3.4 Unsaturated methylated BHTs. The summed mass chromatogram for the unsaturated 3MeBHT showed two pairs of peaks at 20.0 and 20.2 min (peaks m and n) and at 21.2 and 21.4 min (peaks o and p) (Fig. 1E). The MS^2 spectra of peaks m and n (Fig. S2b) showed very similar fragmentation to the Δ^6-unsaturated BHTs, with the expected +14 Da offsets in the A and B ring fragments. The fragments in the middle mass range were largely absent. The spectra of peaks o and p (Fig. S2c) showed the same series of C_{20} to C_{26} fragments as observed for the two unsaturated BHT peaks (g and h) designated as Δ^{11}. Based on the relative retention times and similarities of their spectra to the unsaturated BHTs, we identify these peaks as (m) Δ^6-3MeBHT-22*R*,34*S*, (n) Δ^6-3MeBHT-22*R*,34*R*, (o) Δ^{11}-3MeBHT-22*R*,34*S*, and (p) Δ^{11}-3MeBHT-22*R*,34*R*. All but Δ^6-3MeBHT-22*R*,34*R* were also reported by Peiseler and Rohmer (1992) in *K. xylinus.*

We also detected two isomers of di-unsaturated 3Me-BHT at 19.00 and 19.12 min (Fig. 1F, peaks q and r). Peiseler and Rohmer (1992) also detected two isomers of $\Delta^{6,11}$ -3MeBHT in *K. xylinus*, differing in stereochemistry at the C-34. Based on this and the relative retention times we identify peaks q and r as $\Delta^{6,11}$-3MeBHT-22*R*,34*S* and $\Delta^{6,11}$-3MeBHT-22*R*,34*R*, respectively. The observed fragmentation spectrum (Fig. S2d) closely matched those of $\Delta^{6,11}$-BHT. It is noteworthy that the fragment at *m/z* 203 (analogous to *m/z* 189 in the MS^2 spectrum of $\Delta^{6,11}$-BHT) is diagnostic for a di-unsaturated MeBHT and not for Δ^6-MeBHT as is the case with EI ionization. However, the *m/z* 203 fragment alone is not sufficient to identify a $\Delta^{6,11}$-MeBHT as a fragment with identical *m/z* is also present in the fragmentation spectrum of Δ^6-BHT, although it is generated via a different fragmentation pathway.

3.3.5. Bacteriohopanepentols and -hexols. In order to establish elution and fragmentation patterns for bacteriohopanepentol and -hexol (BHpentol and BHhexol, respectively), as well as their 3Me-homologues, we analyzed an extract of '*Ca.* M. oxyfera' (Kool et al., 2014). Fig. 4A shows summed mass chromatograms revealing the presence of BHT (peak a), BHpentol

(peak b) and BHhexol (peak c) and their methylated analogues (peaks d, e, and f). The BHPs elute in reversed order of number of hydroxylations on the side chain. Whereas ammoniation is the preferred ionization for BHT, the balance shifts towards protonation for BHhexol (Table S1). Fig. 4D shows the MS^2 spectra of the protonated molecule ($[M+H]^+$) of BHhexol. The observed fragmentation pattern is comparable to the one described above for BHT, with major fragments representing losses of 1 to 5 hydroxyl moieties at *m/z* 561.451 ($C_{35}H_{61}O_5^+$, Δ ppm -0.86), 543.441 ($C_{35}H_{59}O_4^+$, Δ ppm -0.14), 525.431 ($C_{35}H_{57}O_3^+$, Δ ppm 1.65), 507.421 ($C_{35}H_{55}O_2^+$, Δ ppm 0.16), and 489.406 ($C_{35}H_{53}O^+$, Δ ppm -6.65), respectively. The base peak is the diagnostic ion for BHPs at *m/z* 191.179 ($C_{14}H_{23}^+$, Δ ppm -1.50). The fragment at *m/z* 369.353 ($C_{29}H_{49}^+$, Δ ppm -2.51) representing the ring system after loss of the side chain is only present in very low abundance (<5%), but instead a fragment at *m/z* 397.383 ($C_{29}H_{49}^+$, Δ ppm 0.31) is formed with the cleavage apparently occurring at the C-22/C-30 bond. Similar to what was observed for BHT, we observe several fragments at *m/z* 297.222 ($C_{21}H_{29}O$, Δ ppm 3.56), *m/z* 315.233 ($C_{21}H_{31}O_2$, Δ ppm 2.96), *m/z* 333.243 ($C_{21}H_{33}O_3$, Δ ppm 1.59) and *m/z* 351.253 ($C_{21}H_{35}O_4$, Δ ppm -0.33), which based on their assigned elemental composition, appear to be complimentary to the ion at *m/z* 191 (A and B ring) and represent the remainder of the ring system and the side chain with 0 to 4 hydroxyl moieties.

The MS^2 spectrum of the ammoniated molecule for BHpentol (Fig. 4C) shows the same characteristics as discussed for BHT and BHhexol. 3MeBHpentol and 3MeBHhexol elute ca. 2 min after and fragment similarly to their non-methylated counterparts, generating a.o. the diagnostic fragment at *m/z* 205 and with all ions containing the A-ring shifted by +14 Da (see Fig. S3 for mass spectra).

3.3.6. Aminobacteriohopanepolyols. Mass chromatograms of the protonated molecules of aminotriol, -tetrol, and -pentol (Fig. 5A; peaks a, b, c, and d, respectively), as well as their 3Me-counterparts (Figure 5B; peaks e, f, and g, respectively) show their distribution in *M.*

capsulatus, a well-studied bacterium producing these aminoBHPs (e.g., Neunlist and Rohmer, 1985b; Talbot et al., 2001). As expected, the aminoBHPs elute in reversed order of the number of functional groups. The 3Me-aminoBHPs elute ca. 1 to 2.5 min after their corresponding non-methylated counterparts (see Table S1 for exact retention times). Fig. 5A shows a partially resolved, late-eluting isomer of aminotetrol (peak c). Although Talbot et al. (2001) observed a late-eluting isomer to aminotetrol in *Methylocystis parvus*, it has to the best of our knowledge not been observed in *M. capsulatus.*

Talbot et al. (2016) discussed the fragmentation characteristics of non-derivatized aminotriol only and, based on those observations, predicted suitable MRM target ions for (3Me)aminotetrol and (3Me)aminopentol. Here we show MS^2 spectra of aminopentol (Fig. 5C) and 3Me-aminopentol (Fig. 5D) (additional spectra for the aminotriols and -tetrols are shown in Fig. S4; the late eluting isomer of aminotetrol shows similar fragmentation as the main isomer). As was observed by Talbot et al. (2003a) for acetylated aminotriol and Talbot et al. (2016) for non-derivatized aminotriol, fragmentation of the amino-BHPs only occurs with increased collision voltage. Under the conditions used here, i.e., with a stepped collision energy, fragmentation was still limited, but yielded sufficient diagnostic features for positive identification of the full series of aminoBHPs. As is the case with the previous discussed BHPs, the alcohol moieties in the side chain are readily lost as H_2O, yielding a series of fragments at *m/z* 560.467 ($C_{35}H_{62}O_4N^+$, Δ ppm 0.65), *m/z* 542.455 ($C_{35}H_{60}O_3N^+$, Δ ppm -2.99), *m/z* 524.448 ($C_{35}H_{58}O_2N^+$, Δ ppm 0.48), and *m/z* 506.437 ($C_{35}H_{56}ON^+$, Δ ppm 2.19) for aminopentol and *m/z* 574.482 ($C_{36}H_{64}O_4N^+$, Δ ppm -1.09), *m/z* 556.471 ($C_{36}H_{62}O_3N^+$, Δ ppm -1.98), *m/z* 538.462 ($C_{36}H_{60}O_2N^+$, Δ ppm -0.12), and *m/z* 520.450 ($C_{36}H_{58}ON^+$, Δ ppm -2.58) for 3Me-aminopentol. In the lower mass range the diagnostic fragments at *m/z* 191.179 ($C_{14}H_{23}^+$, Δ ppm -3.75) for BHPs and *m/z* 205.195 ($C_{15}H_{25}^+$, Δ ppm -1.40) for MeBHPs are relatively abundant. In addition, there are several N-containing fragments in the mass range

between *m/z* 300 and 400 (Figs. 5C and D, Table S1) that represent the D and E rings with side chain, equivalent to the fragmentation observed for BHPs described above.

3.4 Composite BHPs

3.4.1 Cyclitol ether bacteriohopanetetrol. BHT-CE is a commonly detected, so-called composite BHP (Talbot et al., 2007a). Composite BHPs consist of a linear functionalized side chain bound to a more complex, often polar moiety or head group. In case of BHT-CE, the BHT is ether bound to an amino sugar on the C-35 position (Fig. 6B). Here we analyzed cell material of '*Ca.* Scalindua profunda', in which BHT-CE was previously detected by Rush et al. (2014), to establish elution and fragmentation of this BHP. Fig. 6A shows the mass chromatogram for the $[M+H]^+$ of BHT-CE (*m/z* 708.541). Whereas Rush et al. (2014) detected three isomers of BHT-CE in '*Ca.* S. profunda', eluting closely together, we detected two isomers (Fig. 6A, peak a and b), which could be due to different growing conditions. Fig. 6B shows the MS^2 spectrum of the most abundant isomer, peak b. Talbot et al. (2016) also discussed the fragmentation of non-derivatized BHT-CE, which is very similar to the fragmentation pattern observed here. Fragmentation is limited, but several fragments resulting from loss of up to three hydroxyl moieties are observed at *m/z* 690.529 ($C_{41}H_{72}O_7N^+$, Δ ppm -1.32), *m/z* 672. 529 ($C_{41}H_{70}O_6N^+$, Δ ppm -0.65) and *m/z* 654.508 ($C_{41}H_{68}O_5N^+$, Δ ppm -2.60). In the lower mass range several fragments, representing the intact headgroup (*m/z* 180.087 ($C_6H_{14}O_5N^+$, Δ ppm -0.72)) and the headgroup after loss of several hydroxyl moieties (*m/z* 162.076 ($C_6H_{12}O_4N^+$, Δ ppm -1.45), *m/z* 144.066 ($C_6H_{10}O_3N^+$, Δ ppm -0.62) and *m/z* 126.065 ($C_6H_8O_2N^+$, Δ ppm 0.28)), are observed. Fragments at *m/z* 222.097 ($C_8H_{16}O_6N^+$, Δ ppm -1.37) and *m/z* 204.86 ($C_8H_{14}O_5N^+$, Δ ppm -0.98) appear to consist of the headgroup with two additional carbon atoms from the side chain after fragmentation at the C-33/C-34 bond.

3.4.2 Methylcarbamate-aminoBHPs. A more recently described series of composite BHPs are the methylcarbamate-aminoBHPs (MC-aminoBHPs; Rush et al., 2016). Fig. 7A shows the

series detected in *M. vadi*. The MS^2 spectrum of MC-aminotriol (Fig. 7B; spectra of MC-aminotetrol and –pentol are shown in Fig. S5) showed the predicted losses of up to three hydroxyl moieties as H_2O generating ions at *m/z* 586.483 ($C_{37}H_{64}O_4N^+$, Δ ppm -0.23), 568.474 ($C_{37}H_{62}O_3N^+$, Δ ppm 2.38), and 550.461 ($C_{37}H_{60}O_2N^+$, Δ ppm -2.99). A loss of 32 Da (CH_3OH, representing the methoxy moiety) from the ion at *m/z* 586 to produce m/z 554.456 ($C_{36}H_{60}O_3N^+$, Δ ppm -1.64) was also observed. Losses of 75 Dalton ($C_2H_5O_2N$), representing the methylcarbamate moiety, were observed from the mass peaks at *m/z* 568 or 550 leading to fragment ions at *m/z* 493.438 ($C_{35}H_{57}O^+$, Δ ppm -4.81) and *m/z* 475.430 ($C_{35}H_{55}$, Δ ppm 0.17). These losses were also observed by Rush et al. (2016) after fragmentation of acetylated MC-aminoBHPs. N-containing product ions were observed at *m/z* 76.040 ($C_2H_6O_2N^+$, Δ ppm 9.40), 88.040 ($C_3H_6O_2N^+$, Δ ppm 5.85) and 118.050 ($C_4H_8O_3N^+$, Δ ppm 1.61) and likely represent the methylcarbamate moiety after fragmentation between the nitrogen and C-35, at C-34/C-35, and at C-33/C-34, respectively.

3.5 BHPs in a soil from a terrestrial methane seep

To further examine the performance of the UHPLC-HRMS method for environmental samples with more complex matrices than biomass, we analyzed a soil from a terrestrial methane seep in Sicily (Censo 0 m). A base peak chromatogram is shown in Fig. S6. We were able to detect several of the above discussed BHPs. All detected BHPs are listed in Table S2 and additional MS^2 spectra of BHPs that are not further discussed in the text are shown in supplemental figures. Here we will focus on the description of not previously discussed and new composite BHPs.

3.5.1. AdenosylBHPs. Adenosylhopanes occur ubiquitously in soils (Cooke et al., 2008a, b), yet, adenosylhopane is also an intermediate in BHP side chain synthesis (Bradley et al., 2010)

and the adenosyl-BHPs seem to also have an in situ origin in oxygen minimum zones of the oceans (Kusch et al., 2021). Their occurrence and relative abundance has been used to trace soil organic matter during riverine transport and deposition into the marine environment (Zhu et al., 2011). Three types of adenosylhopanes have been described: type-1, -2, and -3 (see Fig. 9A for general structure; Talbot et al., 2007a; Rethemeyer et al., 2010) of which only the polar head group of adenosylhopane type-1 has been fully identified (Neunlist and Rohmer, 1985a) as adenosine. Adenosylhopane type-2 and -3 show similar fragmentation behavior to type-1, but have an unknown, presumably, nucleoside-type polar head group. Upon fragmentation of adenosylhopanes, a diagnostic fragment, representing the nucleoside, is formed with *m/z* 136 for type-1 (adenosine), *m/z* 151 for type-2, and *m/z* 150 for type-3 (Talbot et al., 2016). Methylated homologues have been observed for each of the three adenosylhopane types (Talbot and Farrimond, 2007; Rethemeyer et al., 2010). Adenosylhopane type-1 and its (di)methylated homologues are the only adenosylhopanes with a known elemental composition and, therefore, searchable based on their exact mass. For adenosylhopanes type-2 and -3, we initially mined the data using a nominal mass approach. This revealed several peaks, of which we then further investigated both the MS^1 and corresponding MS^2 spectra as discussed below.

Fig. 8 shows the full distribution of adenosylhopanes with increasing degree of methylation, as detected in the Censo 0 m soil. The mass chromatogram of the calculated exact mass of the protonated molecule for adenosylhopane type-1 (EC = $C_{40}H_{64}O_3N_5^+$; *m/z* 662.500) revealed a single peak (a) at 22.0 min (Fig. 8A). The MS^2 spectrum (Fig. 9B) contains a single dominant ion at *m/z* 136.062 with an assigned elemental composition of $C_5H_6N_5^+$ (Δ ppm -0.16), confirming the identity of the adenosyl head group. The mass chromatogram of *m/z* 676.516, i.e., the exact mass of the methylated homologue of adenosylhopane type-1, showed a series of four peaks (b through e) (Fig. 8B). Peaks b, c and e all produced the same fragment at *m/z*

136 as found for adenosylhopane type-1, thus indicating the position of the methylation to be on the BHP core. Peaks b, c, and e are therefore likely Me-adenosylhopane type-1, similar to the cluster of three isomers detected by Talbot et al. (2016) in a sediment of River Tyne. Both acetylated and non-derivatized 2MeBHPs elute very closely after their non-methylated counterparts using reversed phase chromatography, while 3MeBHPs elute later (Talbot et al. 2003a, b; 2007a, b; 2016) and as observed here, as discussed above). Based on the elution order and retention time differences compared to adenosylhopane type-1, we identify peak b as 2Me-adenosylhopane type-1, peak e as 3Me-adenosylhopane type-1, and peak c as an unknown Me-adenosylhopane type-1 isomer. This distribution of Me-adenosylhopane type-1 isomers mirrors the distribution of methylated BHTs detected in this soil (see Table S2). Peak d (Fig. 8B) showed an MS^2 spectrum with a single fragment at *m/z* 150.077 with an assigned elemental composition of $C_6H_8N_5$ (Δ ppm -0.01; Fig. 9C). A fragment ion at *m/z* 150 is diagnostic for adenosylhopane type-3, and in fact Talbot et al. (2016) used the predicted MRM transition of *m/z* 676 to 150 to successfully detect this compound in the River Tyne sediments. We, therefore, identify peak d as adenosylhopane type-3. Based on the AEC, we propose that the polar head group of adenosylhopane type-3 contains a methylated adenine (see Fig. 9C for proposed structure; placement of the methylation is arbitrary).

Fig. 8C shows the mass chromatogram of *m/z* 690.532 (EC = $C_{42}H_{68}O_3N_5^+$) and shows one dominant peak at 25.5 min (h) and two minor earlier eluting peaks (f and g). The MS^2 spectrum of peak f (Fig. 9D) contains two fragments related to the head group, i.e., the base peak at *m/z* 150.077 ($C_6H_8N_5^+$; Δ ppm -0.01) and a fragment at *m/z* 164.093 ($C_7H_{10}N_5^+$, Δ ppm -0.07). This suggests that this peak represents a co-elution of Me-adenosylhopane type-3 and (a minor) adenosylhopane type-3 with a second methylation on the adenine. Talbot et al. (2016) used an MRM transition from *m/z* 690 to 150 and detected a single peak in a sediment from the river Tyne. It is likely that this BHP is similar to the here observed peak f. The MS^2

spectrum of peak g (Fig. 9E) showed a base peak at *m/z* 136.061 (EC = $C_5H_6N_5^+$) and a minor fragment at *m/z* 150.077 ($C_6H_8N_5^+$). We, therefore, propose peak g to represent a co-elution of diMe-adenosylhopane type-1 and Me-adenosylhopane type-3. Peak h again appears to be an adenosylhopane type-3, with an additional methylation on the adenine, based on the product ion at *m/z* 164.093 ($C_7H_{10}N_5^+$; Δ ppm -0.99; Fig.9F), similar to the minor co-elution in peak f.

The mass chromatogram of adenosylhopanes with an EC of $C_{43}H_{70}O_3N_5^+$ (*m/z* 704.547; Fig. 8D) revealed a series of peaks, i, j and k. The MS^2 spectra of all three peaks (shown for peak i in Fig. 9G) show a single fragment at *m/z* 164.093, and therefore we tentatively identify these BHPs as methyl-adenosylhopanes type-3, with an additional methylation on the adenine head group. Peak j also shows minor fragments related to fragmentation in the hopanoid ring system, including *m/z* 191 (Fig. S7A). These BHPs appear to be the core-methylated homologues of peak h, and based on the offset in retention times to peak h, are tentatively identified as a having a methylation at C-2 (peak i), methylation at unknown positon (peak j), and a methylation at C-3 (peak k); a similar distribution as observed for the MeBHTs and the Me-adenosylhopane type-1 peaks.

A search for adenosylhopanes with an EC of $C_{44}H_{72}O_3N_5^+$ (*m/z* 718.563) showed a series of peaks (Fig. 8E) with relative low abundance (two orders of magnitude less than the adenosylhopanes with *m/z* 690.532). Only peak l had an associated MS^2 spectrum, which showed one fragment ion related to the head group at *m/z* 164.093 and minor fragments related to fragmentation in the ring structure (Fig. 7H). We have tentatively identified this BHP as dimethyl-adenosylhopane type-3 with an additional methylation on the adenine head group. Evidence for BHPs methylated at both C-2 and C-3 was previously seen in '*Ca.* Koribacter versatilis', isolated from a pasture soil (Sinninghe Damsté et al., 2017). Adenosylhopanes with *m/z* 732.579 (EC $C_{45}H_{74}O_3N_5^+$) were not detected.

As, in fact, it appears that all adenosylhopanes discussed above are adenosylhopane type-1 with one or two methylations either on the BHP core and/or on the adenine head group, we propose the following new nomenclature for this extended family of adenosylhopanes: methylations on the BHP core are indicated as "(di)Me-adenosylhopane", while methylations on the adenine head group are indicated by a subscript. Adenosylhopane type-1 would thus be simple be named adenosylhopane. Adenosylhopane type-3 would be named adenosylhopane$_{HG\text{-}Me}$ (where the subscript HG refers to head group). The Me-adenosylhopanes with an additional methylation on the adenine (peaks i,j, and k) would be named Me-adenosylhopane$_{HG\text{-}diMe}$, and peak l would be named diMe-adenosylhopane$_{HG\text{-}diMe}$.

As the elemental composition of adenosyl type-2 is unknown, we searched the MS^2 data for the diagnostic fragment ion with a nominal *m/z* of 151 (Talbot et al., 2016). Several signals were found, mostly associated with amino acid lipids such as ornithines, but one MS^2 spectrum (Fig. 10B) clearly showed an adenosylhopane signature, with a single dominant fragment ion at *m/z* 151.061 ($C_6H_7ON_4^+$, Δ ppm -0.38 ppm). Interestingly, this elemental composition matches the EC for N1-methylinosine, which is formed from adenosine via inosine in transfer RNAs, and is found in the RNA of eukaryotes and halo- and thermophilic archaea (Grosjean and Constantinesco, 1996). The EC of the protonated molecule of adenosylhopane type-2 was determined to be $C_{41}H_{65}N_4O_4^+$ (*m/z* 677.500). Fig. 10A shows the mass chromatogram of *m/z* 677.500 from Censo 0 m soil extract with the relatively low abundance peak at 24.24 min from which the MS^2 spectrum was derived. A homologue of the tentatively identified N1-methylinosylhopane, methylated on the BHP core (m/z 691.516; $C_{42}H_{67}N_4O_4^+$), was detected at 24.30 min (peak b, Figs. 10A and S7B). Based on the retention time, we tentatively identify this BHP as 2Me-N1-methylinosylhopane. As N1-methylinosine is formed from adenosine via an initial hydrolytic deamination to inosine, we also searched for the proposed intermediate between adenosylhopane and N1-methylinosylhopane, i.e.,

inosylhopane ($C_{40}H_{63}O_4N_4^+$; *m/z* 663.484). At 20.63 min a peak was identified with an associated MS^2 spectrum showing the predicted head group fragment at *m/z* 137.0458 ($C_5H_5ON_4^+$, Δ ppm -0.20; peak c, Fig. 10A). Minor fragments at *m/z* 529.461 ($C_{35}H_{61}O_3^+$) and *m/z* 511.450 ($C_{35}H_{59}O_2^+$) further confirmed the anhydro-BHT core structure (Fig. 10C).

3.5.2. A novel composite BHP with an N-containing moiety. During a broad search for known BHPs in the Censo 0 m soil, two peaks matching the exact mass and EC of protonated MC-aminotriol and -tetrol (*m/z* 604.494, $C_{37}H_{66}O_5N^+$ and *m/z* 620.488, $C_{37}H_{66}O_6N^+$, respectively) were encountered (Fig. 11A, peaks a and b). However, these peaks elute later than the equivalent BHPs described for *M. vadi* (see above). Although the MS^2 spectra of the peaks detected in the Censo 0 m soil share many characteristics with those of the MC-aminoBHPs, there are several distinct differences. The MS^2 spectrum of peak b (Fig. 11B) is characterized by a series of initial losses of H_2O (-18) from the protonated molecule producing ions at *m/z* 586.483 ($C_{37}H_{64}O_4N^+$, Δ ppm -0.33) , *m/z* 568.474 ($C_{37}H_{62}O_3N^+$, Δ ppm 2.23), *m/z* 550.462 ($C_{37}H_{60}O_2N^+$, Δ ppm -0.23), and *m/z* 532.453 ($C_{37}H_{58}ON^+$, Δ ppm 2.64). However, instead of the characteristic loss of 75 Da, representing the loss of the methylcarbamate, losses of 41 Da (C_2H_3N) and 59 Da (C_2H_5ON) were observed here, generating fragment ions at *m/z* 491.424 ($C_{35}H_{55}O^+$, Δ ppm -2.43) and m/z 473.414 ($C_{35}H_{55}^+$, Δ ppm -1.41), respectively. Dominant N-containing product ions are observed at *m/z* 60.045 ($C_2H_6ON^+$, Δ ppm 4.52) and *m/z* 102.055 ($C_4H_8O_2N^+$, Δ ppm 1.90). The middle *m/z* region shows similar minor fragments, representing the D and E ring and the side chain after loss of the functionalities, as observed for BHpentol. Based on the assigned EC and the fragmentation pattern, we propose this BHP is a composite BHP based on BHpentol bound to an ethenolamine moiety (C_2H_4N) via an ether bond. To the best of our knowledge this composite BHP has not been observed before.

After having tentatively identified this ethenolamine-BHpentol, we identified the BHT and BHhexol homologues (peak a and c, respectively, in Fig. 11A), based on calculated exact

mass and MS^2 fragmentations (Table S3, Figs. S8A and B). Methylated ethenolamine-BHPs were not detected in Censo 0 m, however a BHP matching the calculated exact mass and EC of methylated ethenolamine-BHT ($C_{38}H_{68}O_4N^+$) was detected at 21.44 min (for details see Table S3). The fragmentation pattern was almost identical to what was observed for ethenolamine-BHT (Fig. 11B). However, both diagnostic N-containing product ions were offset by +14 Da resulting in fragments at *m/z* 74.061 ($C_3H_8ON^+$, Δ ppm 9.446), and *m/z* 116.071 ($C_5H_{10}O_2N^+$, Δ ppm 3.575) (Fig. S8C). No diagnostic losses could be observed in this case. This BHP was, therefore, tentatively identified as a propenolamine-BHT. A butenolamine homologue was not detected.

3.5.3 Acylated ethenolamines. Using the exact mass of the most common diagnostic ion for BHPs, i.e., *m/z* 191.179 ($C_{14}H_{23}^+$), the MS^2 data was investigated for other potential unknown BHPs. This revealed the presence of a series of late eluting (35-40 min) compounds with *m/z* values >800 (Fig. S9). One of the most abundant of these unknowns was a compound with *m/z* 840.743 and an assigned EC of $C_{54}H_{98}O_5N^+$ (Δ ppm -1.54). A mass chromatogram for this EC showed a cluster of peaks consisting of at least eight isomers (peaks a to h, Fig. 12A) with near identical MS^2 spectra. Fig. 12B shows the MS^2 spectrum of the most abundant peak e. Two losses of H_2O are observed from the parent ion resulting in fragment ions at *m/z* 822.733 ($C_{54}H_{96}O_4N^+$, Δ ppm -0.26) and *m/z* 804.720 ($C_{54}H_{94}O_3N^+$, Δ ppm -0.46). In the middle region of the mass spectrum a cluster of fragment ions are observed, which are formed after an initial loss of 252.246 ($C_{17}H_{32}O$, Δ ppm 0.81) from the parent ion and further losses of -18 Da (H_2O) and, interestingly, -41 Da (C_2H_3N) and -59 Da (C_2H_5ON), similar to the fragmentation pattern observed for the earlier described ethenolamine BHPs. Indeed, the diagnostic product ions of this novel class of BHPs at *m/z* 60 and 102 were also present. Based on the resemblance of the MS^2 spectrum to that of ethenolamine-BHT and the loss of a $C_{17}H_{32}O$ moiety, we tentatively identified this compound as a $C_{17:0}$-*N*-acyl-ethenolamine-BHT

(Fig. 12B). The fatty acid moiety can, based on the data here, only be identified to the level of carbon number and double bond equivalent. Several causes are possible for the multitude of isomers. The head group can be bound to the polyol tail of the BHP at different positions (C-32, C-33, C-34, or C-35), and/or by isomery within the BHT core structure, or by structural differences (linear vs. branched) in the fatty acid tail.

In addition to the $C_{17:0}$-*N*-acyl-ethenolamine-BHTs, we detected complex distributions of $C_{15:0}$ to $C_{18:0}$-*N*-acyl-ethenolamine-BHTs (Fig. S9). $C_{14:0}$- and $C_{19:0}$-*N*-acyl-ethenolamine-BHTs appeared only present at trace levels and could not be confirmed by obtaining MS^2 spectra. A full listing by retention time, for those isomers confirmed by MS^2, is given in Table S2. Ethenolamine-BHTs bound to $C_{15:0}$ and $C_{17:0}$ fatty acids were most abundant in the Censo 0 m soil, but the $C_{16:0}$ bound ethenolamine BHTs showed the most complex distribution with 12 isomers confirmed by MS^2 spectra. A search for unsaturated homologues resulted in the detection of ethanolamine-BHTs bound to $C_{17:1}$ and $C_{18:1}$ fatty acids (Table S2, Fig. S10), which were only present at trace levels. Acylated ethenolamine-BHTs comprising an unsaturated hopanoid core were not detected. Acylated ethenolamine-BHPs based on BHpentol and BHhexol were also detected (Table S2, Fig. S10) and comprised $C_{15:0}$ to $C_{18:0}$, and $C_{17:1}$ and $C_{18:1}$ N-bound acyl moieties, i.e., comparable with the distribution of the ethenolamine-BHTs. Interestingly, many more isomers were identified for ethenolamine-BHhexol than for ethenolamine-BHpentol, while BHhexol itself was not detected.

3.5.4 Acylated aminotriols.

A further search for acylated BHPs revealed a series of *N*-acyl-aminotriols in the Censo 0 m soil (Fig. S11). HPLC-MS detection of derivatized *N*-acyl-aminotriols was previously reported by Talbot et al. (2007a) in *Nitrosomonas europaea* and *Rhodomicrobium vannielii*. However, the MS^2 spectrum (shown for $C_{14:0}$-*N*-acyl-aminotriol, Fig. 13) of the non-derivatized molecule proves to be much more diagnostic than that produced from the

derivatized molecule. Here, three losses of H_2O are observed from the parent ion resulting in fragment ions at *m/z* 738.676 ($C_{49}H_{86}O_2N^+$, Δ ppm 0.04), *m/z* 720.663 ($C_{49}H_{86}O_2N^+$, Δ ppm -3.078) and *m/z* 702.658 ($C_{49}H_{84}ON^+$, Δ ppm -3.17). Loss of 210.199 Da ($C_{14}H_{26}O$, Δ ppm 4.07) leads to a product ion at *m/z* 546.486 ($C_{35}H_{64}O_3N^+$, Δ ppm 4.07), matching the $[M+H]^+$ of aminotriol. Further fragmentation indeed matches the fragmentation for amino BHPs as described earlier, although fragment ions in the lower mass region appear more abundant here. The acyl moiety is easily defined by a prominent fragment ion at *m/z* 228.232 ($C_{14}H_{30}ON^+$, Δ ppm -4.12). An additional N-containing fragment ion is observed at *m/z* 270.243 ($C_{16}H_{32}O_2N^+$, Δ ppm -3.01) and is likely formed after cleavage of the C-33/C-34 bond.

Whereas Talbot et al. (2007a) reported aminotriol acylated to $C_{16:0}$ and $C_{16:1}$ FAs in *N. europaea* and to $C_{18:0}$, $C_{18:1}$, and $C_{19:0}$ in *R. vannieli*, we detect aminotriols acylated with much shorter chain fatty acids ranging from $C_{8:0}$ to $C_{18:0}$ FA, with the $C_{11:0}$-*N*-acyl-aminotriol being the most abundant homologue (peak d, Fig. S11). In addition, aminotriols acylated to $C_{11:1}$, $C_{12:1}$, $C_{14:1}$ and $C_{16:1}$ fatty acids were detected (Table S2). *N*-acyl-aminotetrols were not detected, and only trace levels of a $C_{16:0}$-N-acyl-aminopentol were detected in the Censo 0 m soil (Fig. S12). A complicating factor in identifying the full spectrum of acyl-BHPs is the fact that there is a considerable overlap in elemental composition between the acyl-ethenolamine-BHPs with the *N*-acyl-aminoBHPs. For illustration, the $[M+H]^+$ of an aminotetrol bound to a $C_{17:1}$ FA has an elemental compositions of $C_{52}H_{94}O_5N^+$, which is identical to that of an ethenolamineBHT bound to a $C_{15:0}$ FA. It is, therefore, important to evaluate the fragmentation of each detected compound.

3.5.5 Multi-conjugated composite aminotriols. While charting the full inventory of *N*-acyl-aminotriols, we also encountered several compounds that were clearly related to the *N*-acyl-aminotriols as evident from their MS^2 spectra (e.g., Fig. 14B). The most abundant of these

was a compound revealed in a mass chromatogram of *m/z* 932.719 (Fig. 14A, peak a) and an assigned EC of the protonated molecule $C_{55}H_{98}O_{10}N^+$ (Δ ppm -1.07). An initial loss of 176 ($C_6H_8O_6$) yields a base peak at *m/z* 756.685 with an assigned EC matching that of $C_{14:0}$-*N*-acyl-aminotriol ($C_{49}H_{90}O_4N^+$, Δ ppm -1.42). The initial loss of 176 Da matches the predicted loss and EC for a glucuronic acid moiety. Further fragmentation was identical to that observed for $C_{14:0}$-*N*-acyl-aminotriol, revealing the aminotriol core at *m/z* 546 and the $C_{14:0}$ fatty acid moiety at *m/z* 228. The MS^2 spectrum of peak b is identical to that of peak a, and peak b thus probably reflects an isomer. Although glucuronic acid is not a very common head group in intact polar lipids, it has been observed in bacteria, fungi, and plants (e.g., Bosak et al., Burugupalli et al., 2020; Fontaine et al., 2009; Hölzl and Dörmann, 2007; Wang et al., 2020). The stereochemistry of the glucuronic acid was not confirmed here and therefore we tentatively identify these compounds as $C_{14:0}$-*N*-acyl-glycuronyl-aminotriols (Fig. 14B). In addition to the $C_{14:0}$-*N*-acyl-glycuronyl-aminotriol, a $C_{15:0}$-*N*-acyl-glycuronyl-aminotriol was also detected (Table S2). To the best of our knowledge this is the first report of BHPs with conjugations on more than one position on the BHP core.

4. Conclusions

We have shown the applicability of UHPLC-ESI/$HRMS^2$ for the analysis of non-derivatized BHPs in both microbial cultures as well as environmental samples. The chromatographic system used here allows separation of a broad range of BHPs, ranging from the relatively simple BHPs to nitrogen-containing BHPs and complex composite BHPs. Furthermore, isomers are readily separated. Identification is achieved based on diagnostic spectra, that contain information on the BHP core structure, the functionalized tail, as well as bound moieties. For the first time, we established the elemental composition of the nucleobase of adenosylhopanes type-2 and type-3, showing that in fact, all adenosylhopanes identified so far are modifications of adenosyl either by one or two methylations on the adenine head group

(type-3) or by deamination followed by methylation (type-2). Furthermore, we have demonstrated the usefulness of HRMS in the identification of novel composite BHPs. We have tentatively identified several new composite BHPs in a soil (e.g., the (*N*-acyl-)ethanolamine-BHPs), showing a previously unobserved diversity and complexity in existing BHP structures. The analytical approach described here allows for simultaneous analysis of the full suite of IPLs, now including BHPs, and represents a further step towards environmental lipidomics. With this method a more complete view of the full assembly of BHPs will be possible. Connecting specific intact BHPs to specific sources and/or geochemical cycles will further aid in the interpretation of their diagenetic products, the geohopanoids, in the geological record. Future work will aim to establish a quantitative protocol for this method using isolated BHPs as well as synthetic internal standards.

Acknowledgements

We thank the associate editor for handling this manuscript and Dr. Kusch and Dr. Lipp for their helpful comments and suggestions. This work was funded by Netherlands Earth System Science Center (NESSC) through a Gravitation grant to JSSD (grant no. 024.002.001) from the Dutch Ministry for Education, Culture and Science, NWO middelgroot grant no. 834.13.004 to ECH, and a Natural Environment Research Council (NERC; United Kingdom) grant to DR (project ANAMMARKS (NE/N011112/1)). This project also received funding from the European Research Council (ERC) under the European Union's Horizon 2020 research and innovation program (grant agreement No 694569-MICROLIPIDS) to JSSD. Cultures were kindly provided by H. Hirayama (JAMSTEC), G.H.L. Nuijten, O. Rasigraf, and M.S.M. Jetten (Radboud University), M. Rohmer and P. Schaeffer (Strasbourg University). We thank F. Grassa (INGV) for assistance to NS during field work.

References

Bale, N.J., Villanueva, L., Hopmans, E.C., Schouten, S., and Sinninghe Damsté, J.S., 2013. Different seasonality of pelagic and benthic Thaumarchaeota in the North Sea, Biogeosciences 10, 7195–7206.

Bale, N.J., Sorokin, D.Y., Hopmans, E.C., Koenen, M., Rijpstra, W.I.C., Villanueva, L., Wienk, H., Sinninghe Damsté, J.S., 2019. New insights into the polar lipid composition of extremely halo(alkali)philic euryarchaea from hypersaline lakes. Frontiers in Microbiology 10, 377.

Besseling, M.A., E. C. Hopmans, R. Christine Boschman, J. S. Sinninghe Damsté, Villanueva, L., 2018. Benthic archaea as potential sources of tetraether membrane lipids in sediments across an oxygen minimum zone. Biogeosciences 15, 4047–4064.

Bligh, E.G., Dyer, W.J., 1959. A rapid method of total lipid extraction and purification. Canadian Journal Biochemistry Physiology 37, 911-917.

Blumenberg, M., Seifert, R., Michaelis, W., 2007. Aerobic methanothrophy in the oxic-anoxic transition zone of the Black Sea water column. Organic Geochemistry 38, 84-91.

Bosak, T., Schubotz, F., de Santiago-Torio, A., Kuehl, J.V., Carlson, H.K., Watson, N., Daye, M., Summons, R.E., Arkin, A.P., Deutschbauer, A.M., 2016. System-wide adaptations of *Desulfovibrio alaskensis* G20 to phosphate-limited conditions. PLOS ONE 11: e0168719.

Burugupalli, S., Almeida, C.F., Smith, D.G.M, Shah, S., Patel, O., Rossjohn, J., Uldrich, A.P., Godfrey, D.I. ,Williams, S.J., 2020. α-Glucuronosyl and α-glucosyl diacylglycerides, natural killer T cell-activating lipids from bacteria and fungi. Chemical Science 11, 2161-2168.

Bradley, S.A., Pearson, A., Sáenz, J.P., Marx, C.J., 2010. Adenosylhopane: The first intermediate in hopanoid side chain biosynthesis. Organic Geochemistry 41, 1075-1081.

Cooke, M.P., Talbot, H.M., Wagner, T., 2008a. Tracking soil organic carbon transport to continental margin sediments using soil-specific hopanoid biomarkers: A case study from the Congo fan (ODP site 1075). Organic Geochemistry 39, 965–971.

Cooke, M.P, Talbot, H.M., Farrimond, P., 2008b. Bacterial populations recorded in bacteriohopanepolyol distributions in soils from Northern England. Organic Geochemistry 39, 1347–1358.

Cooke, M.P., van Dongen, B.E., Talbot, H.M., Semiletov, I., Shakhova, N., Guo, L., Gustafsson, O., 2009. Bacteriohopanepolyol biomarker composition of organic matter exported to the Arctic Ocean by seven of the major Arctic rivers. Organic Geochemistry 40, 1151–1159.

Costantino, V., Fattorusso, E., Imperatore, C., Mangoni, A., 2000. The first 12-methylhopanetetrol from the marine sponge *Plaktoris simplex*. Tetrahedron 56, 3781-3784.

Cvejic, J.H., Bodrossy, L., Kovacs, K.L., Rohmer, M,. 2000a. Bacterial triterpenoids of the hopane series from the methanotrophic bacteria *Methylocaldum* spp.: phylogenetic implications and first evidence for an unsaturated aminobacteriopanepolyol. FEMS Microbiology Letters 182, 361-365.

Cvejic, J.H., Putra, S.R., El-Beltagy, A., Hattori, R., Hattori, T., Rohmer, M., 2000b. Bacterial triterpenoids of the hopane series as biomarkers for the chemotaxonomy of *Burkholderia*, *Pseudomonas* and *Ralstonia* spp.. FEMS Microbiology Letters 183, 295-299.

Etiope, G., Martinelli, G., Caracausi, A., Italiano, F., 2007. Methane seeps and mud volcanoes in Italy: gas origin, fractionation and emission to the atmosphere. Geophysical Research Letters 34, L14303.

Ettwig, K.F., van Alen, T., van de Pas-Schoonen, K.T., Jetten, M.S.M., Strous, M., 2009. Enrichment and molecular detection of denitrifying methanotrophic bacteria of the NC10 phylum. Applied and Environmental Microbiology 75, 3656–3662.

Fontaine, T., Lamarre, C., Simenel, C., Lambou, K., Coddeville, B., Delepierre, M. Latgé, J-P., 2009. Characterization of glucuronic acid containing glycolipid in *Aspergillus fumigatus* mycelium. Carbohydrate research 344, 1960-1967.

Grassa, F., Capasso, G., Favara, R., Inguaggiato, S., Faber, E., Valenza, M., 2004. Molecular and isotopic composition of free hydrocarbon gases from Sicily, Italy. Geophysical Research Letters 31, L06607.

Grosjean, H., Constantinesco, F., 1996. Enzymatic conversion of adenosine to inosine and to N1-methylinosine in transfer RNAs: A review. Biochimie 78, 488-501.

Hemingway, J. D., Kusch, S., Walter, S. R. S., Polik, C. A., Elling, F. J., Pearson, A., 2018. A novel method to measure the C-13 composition of intact bacteriohopanepolyols, Organic Geochemistry 123, 144–147.

Hirayama, H., Sunamura, M., Takai, K., Nunoura. T., Noguchi, T., Oida, H., Furushima, Y., Yamamoto, H., Oomori, T., Horikoshi, K., 2007 Culture-dependent and -independent characterization of microbial communities associated with a shallow submarine hydrothermal system occurring within a coral reef off Taketomi Island, Japan. Applied and Environmental Microbiology 73, 7642-7656.

Hirayama, H., Fuse, H., Abe, M., Miyazaki, M., Nakamura, T., Nunoura, T., Furushima, Y., Yamamoto, H., Takai, K., 2013. *Methylomarinum vadi* gen. nov., sp nov., a methanotroph isolated from two distinct marine environments. International Journal of Systematic and Evolutionary Microbioly 63, 1073-1082.

Hölzl, G., Dörmann, P., 2007. Structure and function of glycoglycerolipids in plants and bacteria. Progress in Lipid Research 46, 225-243.

Isaac, G., McDonald, S., Astarita, G., 2011. Lipid separation using UPLC with charged surface hybrid technology. Waters Corporation, Milford, MA, USA, internal report.

Murrell, J.C., Dalton, H., 1983., Purification and properties of glutamine synthetase from *Methylococcus capsulatus* (Bath). Microbiology 129, 1187-1196.

Kool, D.M., Talbot, H.M., Rush, D., Ettwig, K., Sinninghe Damsté, J.S., 2014. Rare bacteriohopanepolyols as markers for an autotrophic, intra-aerobic methanotroph. Geochimica et Cosmochimica Acta 136, 114-125.

Kusch, S., Walter, S., Hemingway, S.R., Pearson, A., 2018. Improved chromatography reveals multiple new bacteriohopanepolyol isomers in marine sediments. Organic Geochemistry 124, 12–21.

Kusch, S., Wakeham, S.G., Sepúlveda, J., 2021. Diverse origins of "soil marker" bacteriohopanepolyols in marine oxygen deficient zones. Organic Geochemistry 151, 104150.

Malott, R.J., Wu, C.-H., Lee, T.D., Hird, T.J., Dalleska, N.F., Zlosnik, J.E.A., Newman, D.K., Speert, D.P., 2014. Fosmidomycin decreases membrane hopanoids and potentiates the effects of colistin on *Burkholderia multivorans* clinical isolates. Antimicrobial Agents and Chemotherapy 58, 5211-5219.

Moore, E.K., Hopmans, E.C., Rijpstra, W.I.C., Villanueva, L., Sinninghe Damsté, J.S., 2016. Elucidation and identification of amino acid containing membrane lipids using liquid chromatography/high-resolution mass spectrometry. Rapid Communications in Mass Spectrometry 30, 739-750.

Nuenlist, S., Rohmer, M., 1985a. A novel hopanoid, 30-(5'-adenosyl)hopane, from the purple non-sulphur bacterium *Rhodopseudomonas acidophila*, with possible DNA interactions. Biochemical Journal 228, 769-771

Nuenlist, S., Rohmer, M., 1985b. Novel hopanoids from the methylotrophic bacteria *Methylococcus capsulatus* and *Methylomonas methanica*. (22S)-35-aminobacteriohopane-30,31,32,33,34-pentol and (22S)-35-amino-3ß-methylbacteriohopane-30,31,32,33,34-pentol. Biochemical Journal 231, 635-639.

Peisler, B and Rohmer, M., 1992. Prokaryotic triterpenoids of the hopane series. bacteriohopanetetrols of new side-chain configuration from *Acetobacter* species. Journal of Chemical Research – Part S 9, 289-299.

Peters, K.E., Moldowan, J.M. 1993. The Biomarker Guide, Prentice Hall, Englewood Cliffs, NJ, USA.

Rethemeyer, J., Schubotz, F., Talbot, H.M., Cooke, M.P., Hinrichs, K.-U., Mollenhauer, G., 2010. Distribution of polar membrane lipids in permafrost soils and sediments of a small high Arctic catchment. Organic Geochemistry 41, 1130–1145.

Ricci, J.N., Coleman, M.L., Welander, P.V., Sessions, A.L., Summons, R.E., Spear, J.R., Newman, D.K. 2014. Diverse capacity for 2-methylhopanoid production correlates with a specific ecological niche. The ISME Journal 8, 675-684.

Rohmer, M., Dastillung, M., Ourisson, G., 1980. Hopanoids from C_{30} to C_{35} in Recent muds - chemical markers for bacterial activity. Naturwissenschaften 67, 456-458.

Rohmer, M., Bouvier-Nave, P., Ourisson, G. 1984. Distribution of hopanoid triterpenes in Prokaryotes. Journal of General Microbiology 130, 1137-1150.

Rohmer, M., Ourisson, G., 1986. Unsaturated bacteriohopanepolyols from *Acetobacter aceti* ssp. *xylinum*. Journal of Chemical Research. Synopses 10, 356 -357.

Rohmer, M. 1993. The biosynthesis of triterpenoids of the hopane series in the Eubacteria: A mine of new enzyme reactions. Pure and Applied Chemistry 65, 1293-1298.

Rush, S., Sinninghe Damsté, J.S., Poulton, S.W., Thamdrup, B., Garside, A.L., González, J.A., Schouten, S., Jetten, M.S.M., Talbot, H.M. 2014. Anaerobic ammonium-oxidising bacteria: A biological source of the bacteriohopanetetrol stereoisomer in marine sediments. Geochimica et Cosmochimica Acta 140, 50-64.

Rush, D., Osborne, K.A., Birgel, D., Kappler, A., Hirayama, H., Peckmann, J., Poulton, S.W., Nickel, J.C., Mangelsdorf, K., Kalyuzhnaya, M. Sidgwick, F.R., Talbot, H.M. 2016. The

bacteriohopanepolyol inventory of novel aerobic methane oxidizing bacteria reveals new biomarker signatures of aerobic methanothropy in marine systems. PLoS ONE 11, e0165635.

Sáenz, J.P., Wakeham, S.G., Eglinton, T.I., Summons, R.E. 2011. New constraints on the provenance of hopanoids in the marine geologic record: Bacteriohopanepolyols in marine suboxic and anoxic environments. Organic Geochemistry 42, 1351-1362.

Schulenberg-Schell, H., Neuss, B., Sahm, H.1989. Quantitative determination of various hopanoids in microorganisms. Analytical Biochemistry 181, 120-124.

Schwartz-Narbonne, R., Schaeffer, P., Hopmans, E.C., Schenesse, M., Charlton, E. A., Jones, D. M., Sinninghe Damsté, J.S., Ul Haque, M.F., Jetten, M.S.M., Lengger, S.K., Murrell, J.C., Normand, P., Nuijten, G.H.L., Talbot, H.M., Rush, D. 2020. A unique bacteriohopanetetrol stereoisomer of marine anammox. Organic Geochemistry 143, 103994.

Sessions, A.L., Zhang, L., Welander, P.V., Doughty, D, Summons, R.E., Newman, D.K. 2013. Identification and quantification of polyfunctionalized hopanoids by high temperature gas chromatography–mass spectrometry. Organic Geochemistry 56, 120-130.

Simonin, P., Tindall, B., Rohmer, M. 1994. Structure elucidation and biosynthesis of 31-methylhopanoids from *Acetobacter europaeus*. European Journal of Biochemistry 225, 765-771.

Sinninghe Damsté, J.S., Rijpstra, W.I.C., Dedysh, S.N., Bärbel U. Foesel, B.U., Villanueva L., 2017. Pheno- and genotyping of hopanoid production in Acidobacteria. Frontiers in Microbiology 8, 968.

Smit, N.T., Rush, D., Sahonero-Canavesi, D.X., Verweij, M., Rasigraf, O., Cruz, S.G., Jetten, M.S.M., Sinninghe Damsté, J.S., Schouten, S., 2019. Demethylated hopanoids in '*Ca*.

Methylomirabilis oxyfera' as biomarkers for environmental nitrite-dependent methane oxidation. Organic Geochemistry 137, 103899.

Smit, N.T., Villanueva, L., Rush, D., Grassa, F., Witkowski, C.R., Holzheimer, M., Minnaard, A.J., Sinninghe Damsté, J.S., Schouten, S., 2021. Novel hydrocarbon-utilizing soil mycobacteria synthesize unique mycocerosic acids at a Sicilian everlasting fire, Biogeosciences 18, 1463–1479.

Sollai, M, Villanueva, L., Hopmans, E.C., Reichart, G.-J., Sinninghe Damsté, J.S., 2019. A combined lipidomic and 16S rRNA gene amplicon sequencing approach reveals archaeal sources of intact polar lipids in the stratified Black Sea water column. Geobiology 17, 91–109.

Sturt, H.F., Summons, R.E., Smith, K., Elvert, M., Hinrichs, K.-U., 2004. Intact polar membrane lipids in prokaryotes and sediments deciphered by high performance liquid chromatography/ electrospray ionization multistage mass spectrometry – new biomarkers for biogeochemistry and microbial ecology. Rapid Communications in Mass Spectrometry 18, 617-628.

Talbot, H.M., Watson, D.F., Murrell, J.C., Carter, J.F., Farrimond, P., 2001. Analysis of intact bacteriohopanepolyols from methanotrophic bacteria by reversed-phase high-performance liquid chromatographyatmospheric pressure chemical ionization mass spectrometry. Journal of Chromatography A 921, 175-185.

Talbot, H.M., Squier, A.H., Keely, B.J., Farrimond, P., 2003a. Atmospheric pressure chemical ionisation reversed-phase liquid chromatography/ion trap mass spectrometry of intact bacteriohopanepolyols. Rapid Communications in Mass Spectrometry 17, 728–737.

Talbot, H.M., Summons, R., Jahnke, L., Farrimond, P., 2003b. Characteristic fragmentation of bacteriohopanepolyols during atmospheric pressure chemical ionization liquid

chromatography/ion trap mass spectrometry. Rapid Communications in Mass Spectrometry 17, 2788–2796.

Talbot, H.M., Watson, D.F., Pearson, E.J., Farrimond, P., 2003c. Diverse biohopanoid compositions of non-marine sediments, Organic Geochemistry 34, 1353-1371.

Talbot, H.M., Rohmer, M., Farrimond, P. 2007a. Rapid structural elucidation of composite bacterial hopanoids by atmospheric pressure chemical ionization liquid chromatography/ion trap mass spectrometry. Rapid Communications in Mass Spectrometry 21, 880–892.

Talbot H.M., Rohmer, M., Farrimond, P., 2007b. Structural characterisation of unsaturated bacterial hopanoids by atmospheric pressure chemical ionization liquid chromatography/ion trap mass spectrometry. Rapid Communications in Mass Spectrometry 21, 1613–1622.

Talbot, H.M., Farrimond, P., 2007c. Bacterial populations recorded in diverse sedimentary biohopanoid distributions. Organic Geochemistry 38, 1212–1225.

Talbot, H.M, Summons, R.E., Jahnke, L.L., Cockell, C.S., Rohmer, R., Farrimond, P., 2008. Cyanobacterial bacteriohopanepolyol signatures from cultures and natural environmental settings. Organic Geochemistry 39, 232-263.

Talbot, H.M., Sidgwick, F.R., Bischoff, J., Osborn, K.A., Rush, D., Sherry, A, Spencer-Jones, C.L., 2016. Analysis of non-derivatized bacteriohopanepolyols by ultrahigh-performance liquid chromatography/tandem mass spectrometry. Rapid Communications in Mass Spectrometry 30, 2087-2098.

van de Vossenberg, J., Rattray, J.E., Geerts, W., Kartal, B., van Niftrik, L., van Donselaar, E. G., Sinninghe Damsté, J.S., Strous, M., Jetten, M.S.M., 2008. Enrichment and characterization of marine anammox bacteria associated with global nitrogen gas production. Environmental Microbiology 10, 3120–3129.

Wang, H-Y, Tatituri, R.V.V., Goldner, N.K., Dantas, G. Hsu, F-F., 2020. Unveiling the biodiversity of lipid species in *Corynebacteria* - characterization of the uncommon lipid families in *C. glutamicum* and pathogen *C. striatum* by mass spectrometry. Biochimie 178, 158-169.

Welander, P.E., Summons, R.E., 2012. Discovery, taxonomic distribution, and phenotypic characterization of a gene required for 3-methylhopanoid production. Proceedings of the National Acadamy of Sciences 109, 12905-12910.

van Winden, J.F, Talbot, H.M., Kip, N., Reichart, G.-J., Pol, A., McNamara, N.P., Jetten, M.S.M., Op den Camp, H.J.M. Sinninghe Damsté, J.S., 2012. Bacteriohopanepolyol signatures as markers for methanotrophic bacteria in peat moss. Geochimica et Cosmochimica Acta 77, 2012, 52-61.

Wörmer, L., Lipp, J.S., Schröder, J.M., Hinrichs, K.-U., 2013. Application of two new LC–ESI–MS methods for improved detection of intact polar lipids (IPLs) in environmental samples. Organic Geochemistry 59, 10-21.

Wu, C.-H., Kong, L., Bialecka-Fornal, M., Park, S., Thompson, A.L., Kulkarni, G., Conway, S.J. and Newman, D.K., 2015. Quantitative hopanoid analysis enables robust pattern detection and comparison between laboratories. Geobiology 13, 391-407.

Zhu, C. Talbot, H.M., Wagner,T., Pan, J.-M., Pancost, R.D., 2011. Distribution of hopanoids along a land to sea transect: Implications for microbial ecology and the use of hopanoids in environmental studies. Limnology and Oceanography 56, 1850–1865.

Fig. Legends

Fig. 1. Partial mass chromatograms of A: Bacteriohopanetetrol (BHT), B: unsaturated BHT, C: diunsaturated BHT, D: 3MeBHT, E: unsaturated 3MeBHT, and F: di-unsaturated 3MeBHT in *K. xylinus*. All chromatograms represent the summed signals of $[M+H]^+$, $[M+NH_4]^+$ and $[M+Na]^+$. Each trace is labeled with the exact masses used for searching, and the intensity of the highest peak in arbitrary units (AU). All BHT isomers are identified a through r and where applicable labeled with the position of the unsaturation(s) (Δ^6, Δ^{11}, $\Delta^{6,11}$) and the stereochemistry (*S* or *R*) of the C-22 and C-34 position.

Fig. 2. MS^2 spectra of A: Bacteriohopanetetrol (BHT) (peak b, Fig. 1), B: Δ^6-BHT (peak f, Fig. 1), C: Δ^{11}-BHT (peak g, Fig. 1), and D: $\Delta^{6,11}$-BHT (peak j, Fig. 1). Assigned elemental composition of diagnostic mass peaks are listed in Table S1.

Fig. 3. Fragmentation pathways and structures for proposed diagnostic fragments after collision induced fragmentation for BHT, Δ^6- BHT, Δ^{11}- BHT , $\Delta^{6,11}$-BHT, and their 3Me-counterparts.

Fig. 4. Bacteriohopanepolyols in '*Ca.* M. oxyfera'. A: Partial mass chromatograms of BHT (a), BHpentol (b), and BHhexol (c). B: Partial mass chromatograms of 3MeBHT (d), 3MeBHpentol (e), and 3MeBHhexol (f). All chromatograms represent the summed signals of $[M+H]^+$, $[M+NH_4]^+$ and $[M+Na]^+$. Each trace is labeled with the exact masses used for searching and the intensity of the highest peak in arbitrary units (AU). C: MS^2 spectrum of $[M+NH_4]^+$ of BHpentol, and D: MS^2 spectrum of $[M+H]^+$ of BHhexol.

Fig. 5. Aminobacteriohopanepolyols in *M. capsulatus.* A: Partial mass chromatograms of aminotriol (a), aminotetrol (b, c), and aminopentol (d). B. Partial mass chromatograms of 3Me-aminotriol (e), 3Me-aminotetrol (f), and 3Me-aminopentol (g). Each trace is labeled with the exact masses used for searching and the intensity in arbitrary units (AU) of the signal. All

compounds are detected as their $[M+H]^+$. C: MS^2 spectrum of aminopentol, and B: MS^2 spectrum of 3Me-aminopentol. Spectra are partially magnified by the factor indicated.

Fig. 6. Cyclitol ether BHT (BHT-CE) in '*Ca.* Scalindua profunda'. A: Partial mass chromatogram of the $[M+H]^+$ of BHT-CE. The trace is labeled with the exact mass used for searching and the intensity of the highest peak in arbitrary units (AU). B: MS^2 spectrum of BHT-CE. Also shown is the structure of BHT-CE with diagnostic fragmentations indicated.

Fig. 7. Methylcarbamate-aminoBHPs (MC-aminoBHPs) in *M. vadi*. A: partial mass chromatograms of the $[M+H]^+$ of MC-aminopentol (a), -aminotetrol (b) and -aminotriol (c). Each trace is labeled with the exact mass used for searching and the intensity in arbitrary units (AU) of the signal. B. MS^2 of MC-aminotriol (mass peak labeled with * result from co-trapping of a co-eluting compound and is not related to this BHP). Also shown is the structure of MC-aminotriol with diagnostic fragmentations indicated.

Fig. 8. Partial mass chromatograms of adenosylhopanes, with increasing number of methylations, in a soil from a terrestrial methane seep (Censo 0 m). Each trace is labeled with the exact mass used for searching, and the intensity of the highest peak in arbitrary units (AU). MS^2 spectra are shown in Fig. 9 if discussed in text; additional MS^2 spectra are shown in Fig. S7 Peaks labeled with '*' are potential isomers, but have no MS^2 spectrum associated.

Fig. 9. Adenosylhopanes detected in Censo 0 m soil. A: General structure of adenosylhopanes, B through H: MS^2 spectra of adenosylhopanes. Proposed structure of the nucleobase is shown with each spectrum. Spectra of peak f (panel D) and peak g (panel E) appear to be mixed spectra of 2 co-eluting adenosylhopanes with identical elemental composition. The nomenclature and structure shown with those spectra is the proposed nucleobase of the major component. Placement of methylations on the nucleobase is arbitrary as the position is unknown.

Fig. 10. Adenosylhopane type-2 in Censo 0 m soil. A: Partial mass chromatograms, (within 2 ppm mass accuracy) of the tentatively identified N1-methylinosinylhopane (peak a), 2-methyl-N1-methylinosinylhopane (peak b), and inosylhopane (peak c), from a soil from an active terrestrial methane seep in Sicily (Censo 0 m). Each trace is labeled with the exact mass used for searching, and the intensity of the highest peak in arbitrary units (AU). B: MS^2 spectrum of N1-methylinosylhopane. C: MS^2 spectrum of inosylhopane. Proposed structures of the inosine based headgroups are shown.

Fig. 11. Novel N-containing composite BHPs in Censo 0 m soil. A. Partial mass chromatograms of a series of novel composite BHPs (a, b, c). Each trace is labeled with the exact mass used for searching, and the intensity of the highest peak in arbitrary units (AU). B. MS^2 spectrum associated with peak b. (mass peak labeled with * results from co-isolation of a co-eluting compound and is not related to this BHP). Also shown is the proposed structure of ethenolamine-BHpentol with diagnostic fragmentations indicated.

Fig. 12. An example of an *N*-acyl-ethenolamine-BHT in Censo 0 m, a soil from a terrestrial methane seep in Sicily. A. Partial mass chromatogram of $C_{17:0}$-*N*-acyl-ethenolamine-BHT. The trace is labeled with the exact mass used for searching, and the intensity of the highest peak in arbitrary units (AU). B. MS^2 spectrum of peak e from panel A with the proposed structure for $C_{17:0}$-*N*-acyl-ethenolamine-BHT with diagnostic fragmentations indicated. Position of the conjugation is arbitrary as the exact position is unknown. The fatty acid moiety is shown with a linear carbon chain, as the exact structure cannot be determined here.

Fig. 13. MS^2 spectrum of $C_{14:0}$-*N*-acyl-aminotriol from Censo 0 m, a soil from a terrestrial methane seep in Sicily. Proposed structure and diagnostic fragmentations are shown. The fatty acid moiety is shown with a linear carbon chain, as the exact structure cannot be determined here. Further details can be found in table S2.

Fig. 14. Novel multi-substituted aminotriol in Censo 0 m, a soil from a terrestrial methane seep in Sicily. A: Partial mass chromatogram of $C_{14:0}$-*N*-acyl-aminotriol with additional glycuronic acid substitution. Trace is labeled with the exact mass used for searching, and the intensity of the highest peak in arbitrary units (AU). B. MS^2 spectrum associated with peak a with proposed structure of $C_{14:0}$-*N*-acyl- glycuronyl-aminotriol with diagnostic fragmentations indicated. Position of the glycuronyl moiety is arbitrary. The fatty acid moiety is shown with a linear carbon chain, as the exact structure cannot be determined here.

Declaration of interests

☒ The authors declare that they have no known competing financial interests or personal relationships that could have appeared to influence the work reported in this paper.

☐The authors declare the following financial interests/personal relationships which may be considered as potential competing interests:

Highlights

- Reversed phase UHPLC-ESI/HRMS^2 detects a broad range of (novel) bacteriohopanepolyols
- BHPs are detected simultaneously with intact polar lipids
- The nucleoside of adenosylhopane type-3 is a methylated adenosine
- The nucleoside of adenosylhopane type-2 is N1-methylinosine

Figure

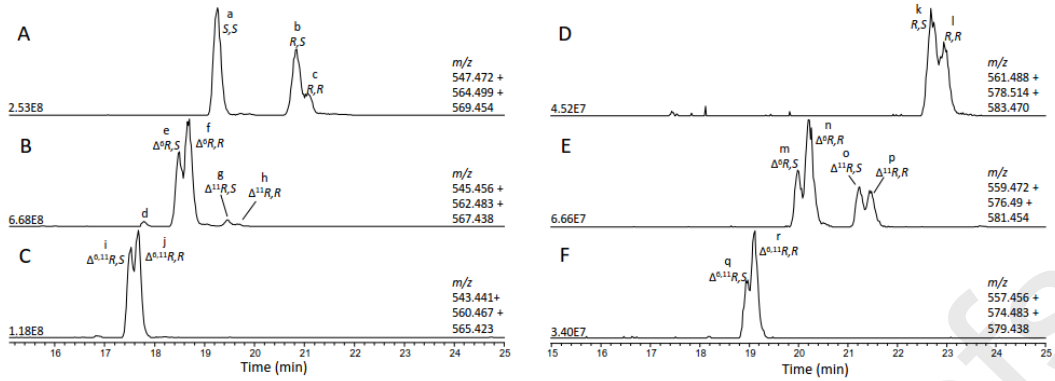

Figure

Click here to access/download;Figure;Figure 2.pptx

A. MS² of *m/z* 564.5, $[M+NH_4]^+$ of BHT (b)

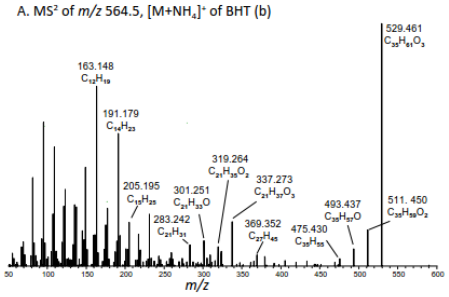

B. MS² of *m/z* 562.5, $[M+NH_4]^+$ of Δ^0- BHT (f)

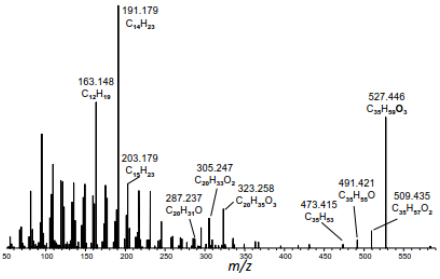

C. MS² of *m/z* 562.5, $[M+NH_4]^+$ of Δ^{11}-BHT (g)

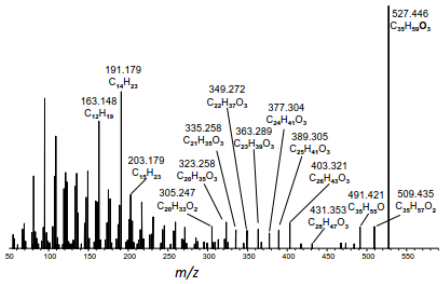

D. MS² of *m/z* 560.5, $[M+NH_4]^+$ of $\Delta^{6,11}$-BHT (j)

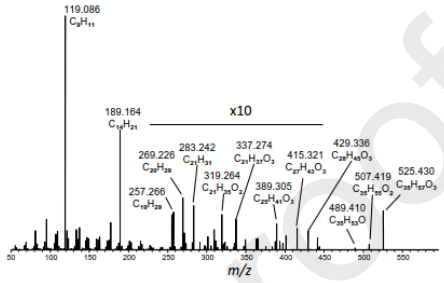

Figure

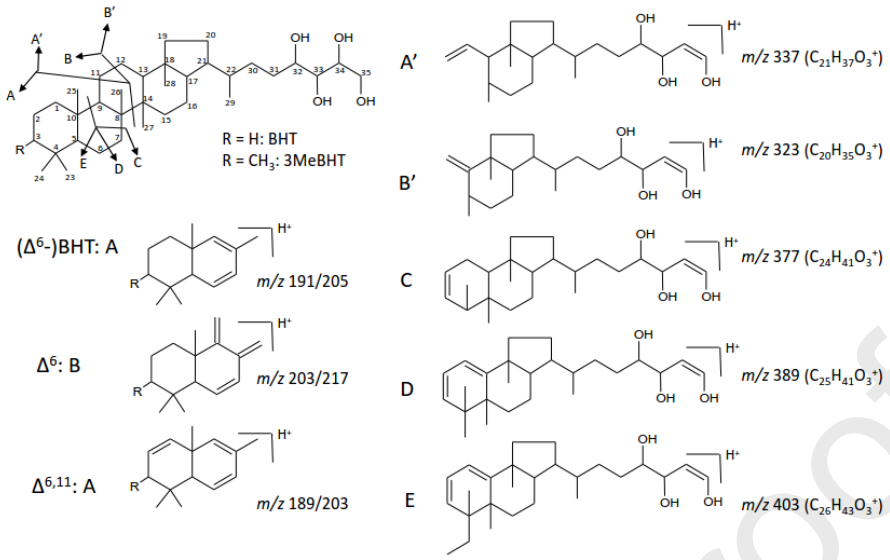

Figure

Click here to access/download;Figure;Figure 4.pptx

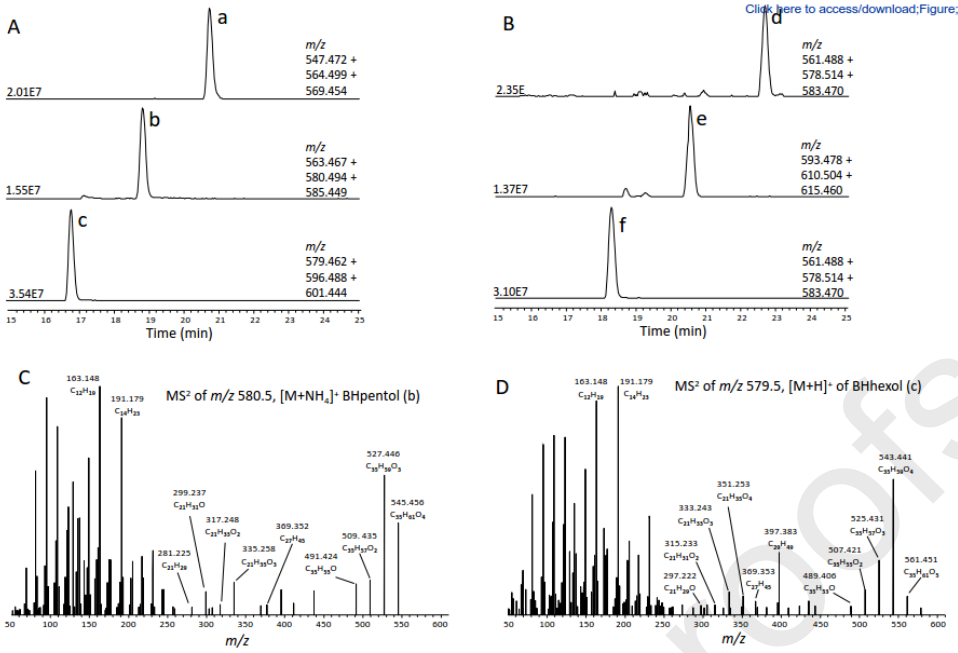

Figure

Click here to access/download;Figure;Figure 5.pptx

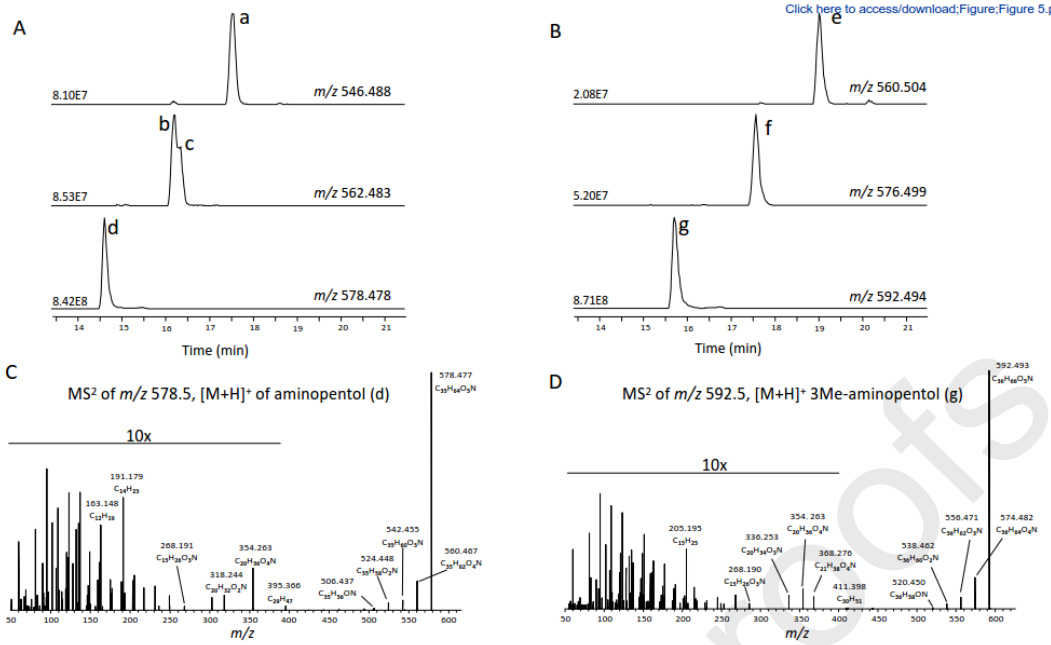

Figure

Click here to access/download;Figure;Figure 6.pptx

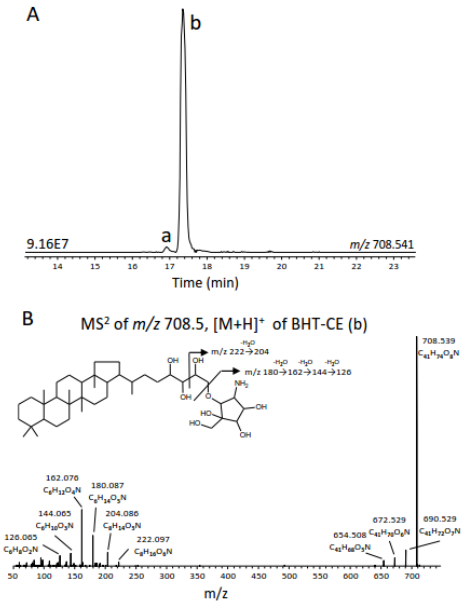

Figure

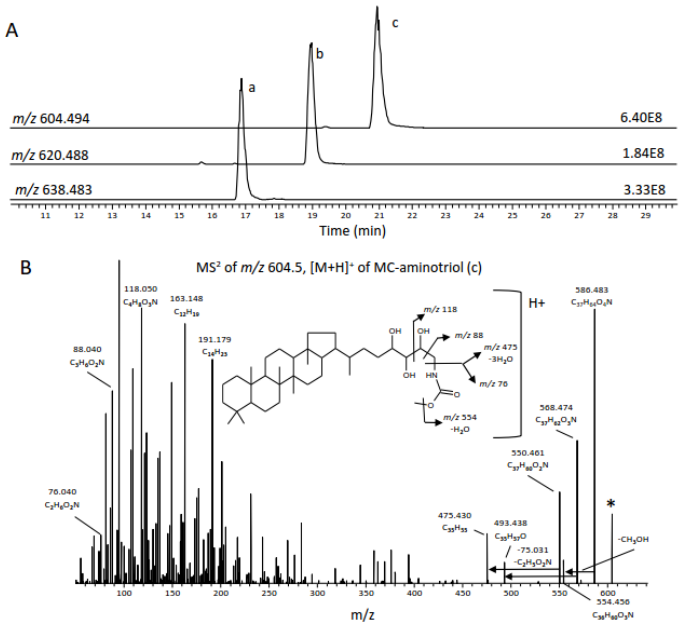

Figure

Click here to access/download;Figure;Figure 8.pptx

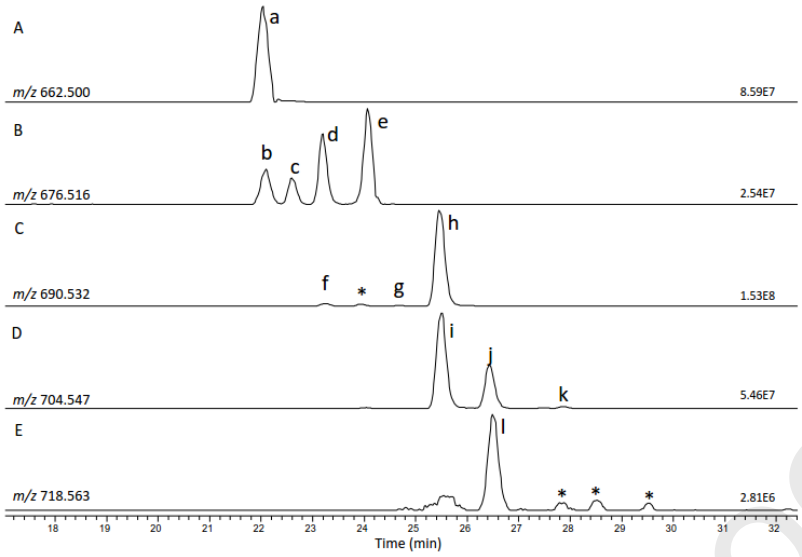

Figure

Click here to access/download;Figure;Figure 9.pptx

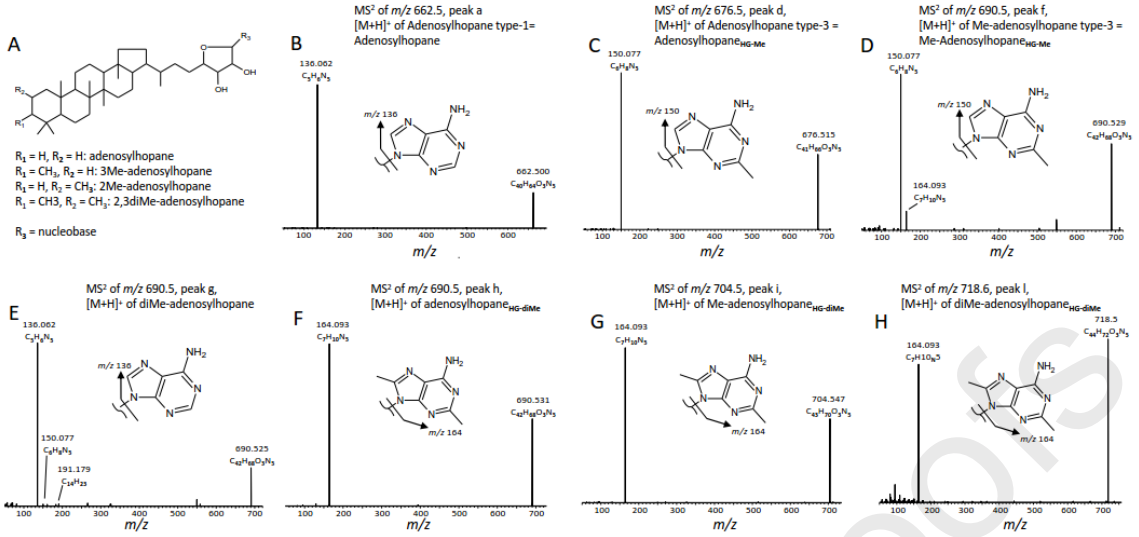

Figure

Click here to access/download;Figure;Figure 10.pptx

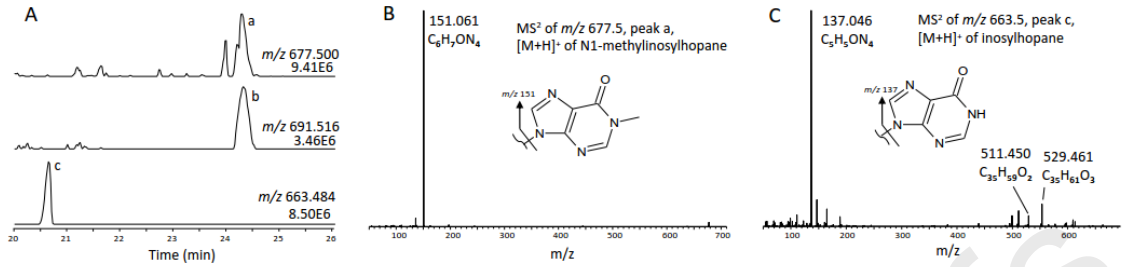

Figure

Click here to access/download;Figure;Figure 11.pptx

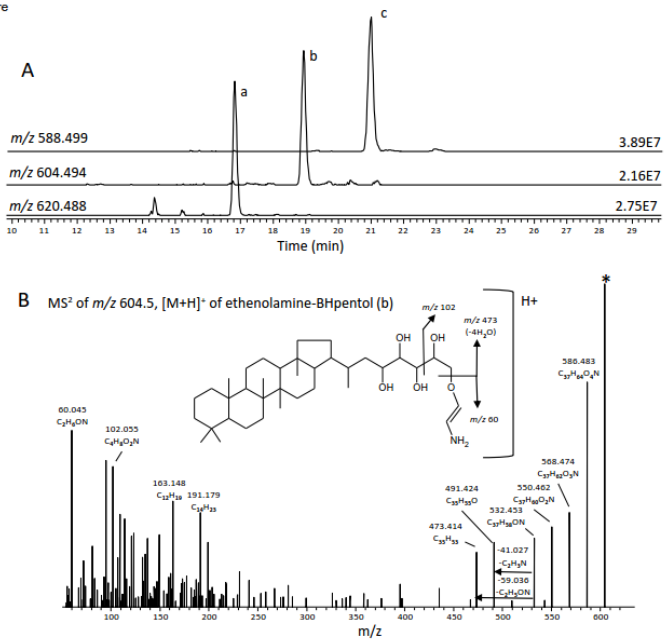

Figure

Click here to access/download;Figure;Figure 12.pptx

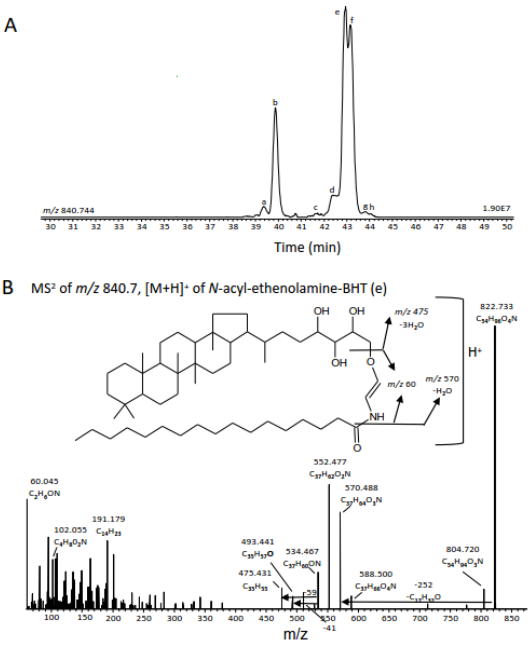

Figure

Click here to access/download;Figure;Figure 13.pptx

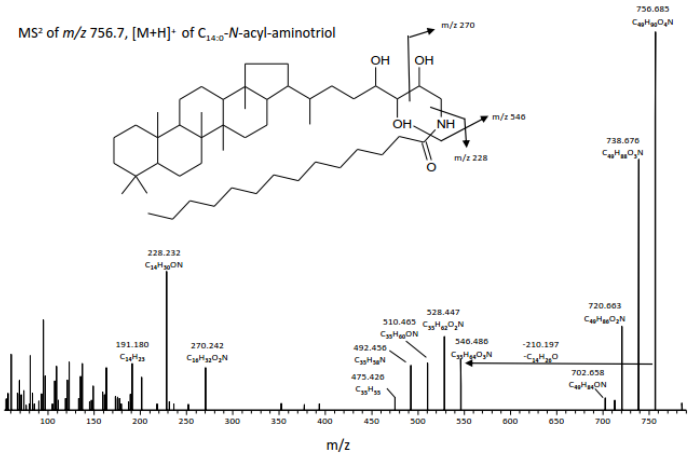

Figure

Click here to access/download;Figure;Figure 14.pptx